COMPARING CLASSIFICATION METHODS FOR MAPPING INVASIVE FLOATING VEGETATION IN THE SACRAMENTO DELTA

A Thesis submitted to the faculty of
San Francisco State University
In partial fulfillment of
the requirements for
the Degree

Master of Science

In

Geographic Information Science

by

Michael Joseph Tarantino

San Francisco, California

December 2019

CERTIFICATION OF APPROVAL

I certify that I have read Comparing Classification Methods for Mapping Invasive Floating Vegetation in the Sacramento Delta by Michael Joseph Tarantino, and that in my opinion this work meets the criteria for approving a thesis submitted in partial fulfillment of the requirement for the degree Master of Science in Geographic Information Science at San Francisco State University.

Leonhard Blesius, Ph.D.
Associate Professor of Geography

Jerry Davis, Ph.D.
Professor of Geography

COMPARING CLASSIFICATION METHODS FOR MAPPING INVASIVE FLOATING VEGETATION IN THE SACRAMENTO DELTA

Michael Joseph Tarantino
San Francisco, California
2019

Water hyacinth (*Eichhornia crassipes*) and water primrose (*Ludwigia hexapetala*) are aggressive invasive floating aquatic vegetation (FAV) species that cause severe economic and ecological impacts to the Sacramento-San Joaquin River Delta in California. These two invasive FAV occupy the same ecological niche within the delta ecosystem and form large floating vegetation mats made up of a mixture of both hyacinth and primrose. Remote sensing methods have proven to be successful in mapping and identifying invasive freshwater aquatic vegetation compared to traditional surveying methods. Using three different types of imagery (multispectral 2019 PlanetScope at 3.7m, multispectral 2018 WorldView-2 at 1.8m, and hyperspectral 2007 AVIRIS at 2.4m) four different remote sensing classification methods were performed to mapping invasive FAV - maximum likelihood (ML), support vector machine (SVM), object-based image analysis (OBIA), and spectral angle mapper (SAM) - resulting in six method/imagery combinations (Planet/ML, Planet/SVM, WorldView-2/ML, WorldView-2/OBIA, AVIRIS/ML, AVIRIS/SAM). The six classifications achieved producer's accuracies from 83% to 91%. The AVIRIS/SAM combination resulted in the highest producer accuracy (91%) and the Planet/SVM combination resulted in the lowest producer accuracy (83%). This study revealed that, when mapping invasive FAV in a freshwater ecosystem, higher spatial resolution results in a higher classification accuracy. This study also revealed that when mapping FAV, hyperspectral imagery results in a higher classification accuracy than multispectral imagery.

I certify that the Abstract is a correct representation of the content of this thesis.

_____ _____

Chair, Thesis Committee Date

ACKNOWLEDGEMENTS

There are several people I would like to thank. I would like to express my deepest gratitude to my thesis advisors, Leonhard Blesius and Jerry Davis. Thank you for your patient guidance, enthusiastic encouragement and constructive critiques of this thesis. I would like to thank my father, Joseph Tarantino, for helping me conduct my thesis fieldwork in the delta. Without his help I would not have been able to rent a motorboat. I would like to thank my partner, Camile Caldwell, for her undying support throughout this entire GIScience master's program and thesis process. I also would like to thank my professors from Cal Poly San Luis Obispo for encouraging me and supporting my decision to pursue my master's degree at San Francisco State University.

TABLE OF CONTENTS

LIST OF TABLES

Table Page

LIST OF FIGURES

Figures Page

1. Introduction

Invasions of aquatic weeds into freshwater, estuarine, wetland, and floodplain habitats decreases biodiversity, threatens critical habitat, alters nutrient cycles, and degrades water quality (Toft et al., 2003). An estimated USD $100 million per year is spent on control and eradication programs targeting invasive aquatic weeds in aquatic ecosystems throughout the United States (Pimentel et al., 2000). Invasive species threaten native species directly through competition and hybridization, and indirectly through ecosystem impacts, such as changing fire regimes, nutrient cycling, hydrology and energy budgets (Mack et al., 2000). Native vegetation in aquatic freshwater environments occupies a vital role in overall environmental function and productivity. Aquatic freshwater vegetation helps to alleviate floods, filter polluted water, and provide habitat for a diverse array of plant and animal species (Zhang et al., 2010). Aquatic freshwater vegetation is an excellent early indicator of physical and chemical degradation in wetland environments as well (Dennison et al., 1993). Livestock grazing, inundation of habitat by dams, groundwater pumping, channelization, and agricultural and urban growth all contribute to the loss of aquatic freshwater ecosystems and areas that manage to remain intact are rapidly invaded by aggressive non-native species. When these non-native species are not properly managed, they out-compete native plants and severely degrade or destroy the wetland habitat (Hestir et al., 2008).

Water hyacinth (*Eichhornia crassipes*) and Uruguay water primrose (*Ludwigia hexapetala*) are aggressive invasive floating aquatic vegetation (FAV) species that cause

severe economic and ecological impacts to the Sacramento-San Joaquin River Delta in California. Invasive water hyacinth and invasive water primrose grow along the islands within the delta channels. These two invasive FAV species occupy the same ecological niche within the delta ecosystem and form large floating vegetation mats made up of a mixture of both hyacinth and primrose (Figure 1). Invasive FAV clogs waterways, impedes recreational activities such as boating and fishing, increases evapotranspiration, decreases biodiversity and changes the functional characteristics of the ecosystem (Toft et al., 2003). Invasive FAV hinder the success of native habitat restoration projects within the Sacramento-San Joaquin River Delta as well (Bossard et al., 2000).

Figure 1. This image was taken on 8/9/2019 during the training sample/ accuracy assessment fieldwork. This image shows the invasive FAV mats, consisting of a mixture of both the round-leaved water hyacinth (right side) and the narrow-leaved water primrose (left side). Photo Credit: Michael Tarantino

Water hyacinth is native to Brazil and has successfully invaded almost every region in the world that is suitable for its growth including China, India, Southeast Asia, Japan, South Africa, Europe, and the United States. Water hyacinth, introduced to the Sacramento River in 1904 by horticulturalists now obstructs navigable waterways, degrades water quality, fouls water pumps, blocks irrigation channels, and causes significant changes to ecological assemblages throughout the Delta (Cohen and Carlton, 1995; Toft et al., 2003). Infamously known as one of the fastest-growing plant species in the world, water hyacinth grows so fast that it can double in size between 6-18 days (Underwood et al., 2006). Water hyacinth floats on top of freshwater as a healthy vegetative canopy with spongy round leaves and produces lavender or white flowers (Figure 2) (CA State Parks, 2018). Water hyacinth spreads easily when broken apart; it can float downstream and form a new colony just from one small clump of separated vegetation (Underwood et al., 2006). Water hyacinth can limit the amount of sunlight that reaches other plants below the surface, interrupting photosynthesis and killing plants and microorganisms important to wildlife. Dead fish have also been seen on top of hyacinth, falling victim to suffocation after jumping on top of the green thickets and being unable to return to the water (Hawkes, 2014). According to the California Dept. of Boating & Waterways, water hyacinth's growth period is typically from spring to late fall and its bloom period is from June to October. For this research study, the analysis time period is the month of August during the peak bloom stage (Hestir et al., 2008).

Figure 2. This image was taken on 8/9/2019 during the training sample/ accuracy assessment fieldwork. This image shows the invasive round-leaved water hyacinth. Photo Credit: Michael Tarantino

Water primrose is the other invasive FAV in the Central Delta that co-occurs with water hyacinth and is equally invasive (Khanna et al., 2011). The invasive species of water primrose found in the delta is native to Uruguay (Boyer and Sutula, 2015). Water primrose has been identified in the Sacramento Delta since the early 2000s and surged after the population crash of the native FAV, pennywort (Khanna et al., 2018). Similar to water hyacinth, water primrose is also floating aquatic vegetation and has the same growth period as water hyacinth (spring - late fall), however during the blooming season (May - December), water primrose produces yellow flowers (Figure 3), while hyacinths bloom are white or lavender. Younger water primrose has oval-shaped leaves and then develops more narrow willow-like leaves as the plant matures (CA State Parks, 2018). It is a perennial herb that grows in moist to flooded areas and although rooted, develops a 2-meter vertical root system that can draw nutrients directly from the water, allowing water primrose to

form floating canopies extending meters into the channel from the shore (CA State Parks, 2018). While their distribution is limited to small patches in their native range, they can grow aggressively and rapidly in their new environment (Haury et al., 2014). Water primrose's fast sexual reproduction, high seed production, successful germination, and the plasticity of morphology contributes to its fast growth rates (Dandelot et al., 2005). These characteristics make water primrose an ideal invasive species capable of engineering ecosystems to benefit its own growth (Dandelot et al., 2005). Like hyacinth, water primrose limits the amount of sunlight that reaches other plants below the surface and interrupts photosynthesis, again leading to killing plants and microorganisms important to wildlife. Water primrose mats also have detrimental effects on human health by providing habitat for mosquitoes transmitting the West Nile virus (Boyer and Sutula., 2015).

Figure 3. This image was taken on 8/9/2019 during the training sample/ accuracy assessment fieldwork. This image shows the invasive narrow-leaved water primrose. Photo Credit: Michael Tarantino

Developing innovative techniques for mapping invasive species is vital to our understanding of invasion ecology and helps to inform management decisions on how to control and monitor invasive activity (Underwood et al., 2006). Traditional terrestrial and aquatic vegetation classification fieldwork requires taxonomic information about vegetation species, previous records of data analysis, and the visual estimation of percentage cover for each species (Adam et al., 2010). Traditional classification methods are labor-intensive, costly, time-consuming, sometimes inapplicable due to the poor accessibility, and often requires direct contact with the plant which can result in further dispersal. Aquatic freshwater vegetation ecosystems are often difficult for field-based mapping methods such as field-based surveying. Due to these restraints, the field-based methods are only practical in relatively small accessible areas (Lee and Lunetta 1996; Hestir et al., 2008). For this research study, a remote sensing approach to vegetation classification is the only way such an assessment can realistically be accomplished, given the rapid ability of these invasive FAV to expand and move.

Mapping invasive vegetation in riparian, wetland, and other freshwater ecosystems with the assistance of remote sensing is an efficient, accurate, and cost-efficient alternative to traditional field mapping methods (Deloach et al., 2005). Remote sensing utilizes satellite imagery to analyze the surface of the earth, providing a synoptic solution for mapping wetland and riparian zones over large spatial areas. In order to make an accurate map, a remote sensing approach to vegetation monitoring and classification must be

accurate, repeatable over space and time, and account for the inherent spatial and environmental heterogeneity of an ecosystem (Hestir et al., 2008).

This invasive FAV identification remote sensing research study uses two types of spectral imagery for classification: multispectral and hyperspectral. Multispectral imagery contains 4-8 spectral bands depending on the satellite and sensor used. Hyperspectral imagery can contain ≥ 200 spectral bands depending on the sensor. Multispectral and hyperspectral imagery data can be processed using remote sensing software for image analysis and cartography purposes. Both multispectral & hyperspectral imagery are used to identify general vegetation classes or to attempt to discriminate invasive vegetation from native vegetation at the species level (Adam et al., 2010; Li et al. 2005). Deciding whether to use multispectral vs. hyperspectral is dependent on the land cover type or object intended for classification, the size of the area of interest, the spatial resolution, as well as the availability of the imagery data.

When classifying vegetation species with remote sensing imagery, a classification analysis is performed. This research study utilized the supervised classification analysis, which allows the user to manually create training areas of pixels within the image to represent the different classification categories. Before a supervised classification is run, the classification algorithm is selected and then the classification begins. This remote sensing research study compares four different classification algorithms to distinguish the most effective algorithm for accurately classifying invasive FAV: Maximum Likelihood (ML); Support Vector Machine (SVM); Object Based Imagery Analysis (OBIA); and

Spectral Angle Mapper (SAM). The ML, SVM, OBIA algorithms are used for classifying multispectral imagery. The ML and SAM classifiers are used for classifying hyperspectral images.

A popular classification algorithm used when performing a supervised classification for identifying aquatic freshwater vegetation is the maximum-likelihood. The maximum likelihood (ML) classifier is a traditional parametric technique for image classification. Because of its widespread and long-time use with established high accuracy, the maximum likelihood classifier is an appropriate control classifier. The ML classification algorithm has proven successful in both hyperspectral and multispectral classifications. This method was utilized when identifying invasive giant reed (*Arundo donax*) along the riverbanks of the Rio Grande in Texas (Deloach et al., 2005).

The support vector machine (SVM) classifier is a pixel-based classification algorithm used when performing a supervised classification for identifying freshwater vegetation. The SVM is an advanced machine learning classification method that is able to process a segmented raster input or a standard image. The SVM classification algorithm yields higher accuracy when using multispectral satellite imagery compared to a SVM using hyperspectral imagery (Abdel-Rahman et al., 2014). The SVM classification is less susceptible to noise and correlated bands as well. SVM is a particularly appealing classification method because of its ability to generalize well even with limited training samples, a common limitation for remote sensing applications. However, this classifier also suffers from parameter assignment issues that can significantly affect obtained results

(Mountrakis et al., 2011). This classification method is performed using multispectral remote sensing software like Erdas Imagine, eCognition, and ArcGIS Pro. SVM has been used in remote sensing-based estimation and monitoring of vegetation biochemical parameters such as chlorophyll concentration, gross primary product, and evapotranspiration (Bazi et al., 2007). A 2014 remote sensing study successfully utilized the SVM classifier to map woodwasp-infested and lightning-struck pine trees in South Africa (Abdel-Rahman et al., 2014). A 2008 study performed a similar SVM-based classification to assess in forest classification accuracy (Huang et al., 2008).

Object-based imagery analysis (OBIA) is another classification method used while performing a supervised classification for identifying freshwater vegetation. The OBIA method is performed on localized neighborhoods of pixels, grouped together with a process called segmentation. The segmentation aspect of OBIA is what makes this classification method different than pixel-based classifiers. Segmentation takes into account both color and shape characteristics of the input imagery when grouping pixels into segmented objects. Since this method uses both shape and color, classified objects resulting from segmentation resemble real-world features because the natural boundaries between land cover types are used as the classified polygon borders, producing cleaner and smoother classification results, which are not pixelated or rasterized. Aquatic freshwater environment OBIA classifications can be challenging due to vegetation cover dynamics with water fluctuation creating rapid and frequent changes in the type, distribution, and density of plant coverage (Belluco et al., 2006). Regardless of the challenges, a 2017

remote sensing study successfully utilized OBIA classification to map wetland vegetation in the Eagle Bay wetland area located at the northern side of Lake Okeechobee in South Florida (Pande-Chhetri et al., 2017). Another remote sensing study from 2008 successfully utilized the object-oriented based classification method to map invasive exotic Australian pine trees in South Florida (Johnson et al., 2008).

Unlike the previous classification methods, the Spectral Angle Mapper (SAM) is specifically used for analyzing hyperspectral imagery. This research classification method is performed using ENVI remote sensing software. The SAM compares the angle between the reference spectra and the pixel, the smaller the angle means the closer the match to the endmember. The reference spectra are the reflectance signatures of the specific vegetation species. The SAM technique uses endmembers derived from the image data that represent different phenological states and geographic locations throughout the dataset, as determined from the field data or regions of interest (ROIs). A 2008 invasive FAV study applied SAM to a subset of the visible and NIR bands to reduce noise contributed to the pixel spectra from mixing with water. The study results revealed that SAM classification is appropriate for species-level monitoring at the regional scale (Hestir et al., 2008).

While there are a number of studies (*e.g. Adam et al., 2010; Ashraf et al., 2010; Belluco et al., 2006; Deloach et al., 2005; DiPietro et al., 2002; Agjee et al., 2015; Hestir et al., 2008; Underwood et al., 2006; Ustin et al., 2006*) using remote sensing technology and methods to map FAV, there are no studies that specifically compare different satellite imagery types as well as different classification methods to determine the most effective

and accurate imagery/algorithm combination for identifying a specific FAV species. Previous studies either performed multiple classification methods (*e.g. Ashraf et al., 2010; Deloach et al., 2005; Hestir et al., 2008; Underwood et al., 2006; Ustin et al., 2006*) on one satellite image, or they would perform one classification method on different types of satellite imagery such as (multispectral vs. hyperspectral) (*e.g. Adam et al., 2010; Belluco et al., 2006; Agjee et al., 2015*). Therefore, the objective of this research is to investigate the most effective method of classifying invasive FAV by comparing different combinations of supervised classification algorithms with different satellite imagery types in order to identify the invasive large floating mats that are formed by a combination of invasive water hyacinth and invasive water primrose.

2. Study Area: Central Sacramento - San Joaquin River Delta

The Sacramento–San Joaquin River Delta is formed by the confluence of the Sacramento and San Joaquin Rivers and drains into the Pacific Ocean through San Francisco Bay. The San Francisco Bay-Delta is the largest estuary in the western United States and its watershed drains over 160,000 km^2 of California. The hydrodynamic heterogeneity of the delta system is constructed in a wide range of salinities, tidal fluxes, water depths, and freshwater inflows with extreme seasonal and inter-annual variability (Hestir et al., 2008). Unfortunately, the delta may have the largest number of invasive species of any estuary in the world (Cohen and Carlton, 1998) and is the focus of a massive coordinated ecosystem restoration program, with direct expenditures exceeding USD $1 billion beginning in the mid-1990s (Lund et al., 2007).

The study area for this invasive FAV identification research study focuses on the Central Sacramento Delta. This region is composed of a maze of meandering channels and inundated delta islands which were created by land reclamation and building of levees in the early 1900s. This has created a diverse system of channels and large expanses of water with varying bathymetry and water velocity (Khanna et al. 2018). The 14.39 km^2 study area for this research project encompasses three major inundated island groups (Figure 4) within the central delta: Sandmound Slough Islands; Little Mandeville Islands; Upper Mildred Islands.

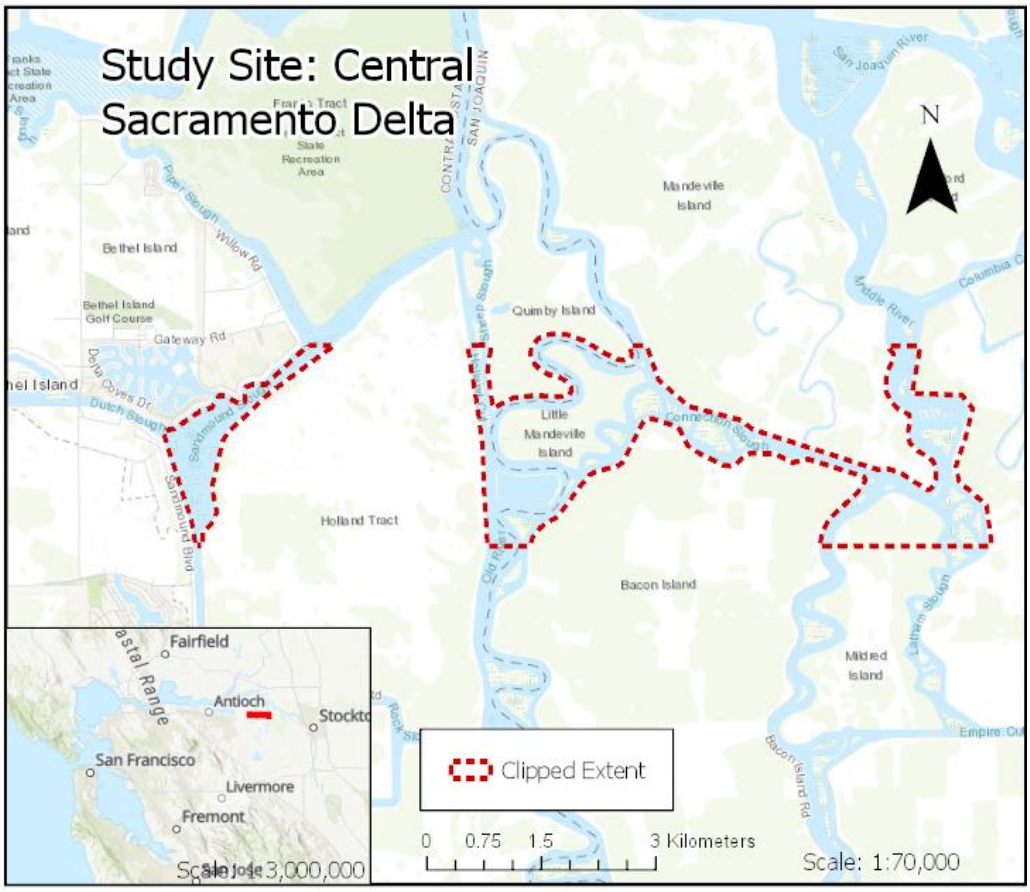

Figure 4. Site map of the 14.39 km^2 clipped extent thesis study area within the Central Sacramento Delta, approximately 90 km NE from San Francisco, CA. GPS fieldwork on these 3 island groups was conducted on 8/9/2019 from 8:30 - 11:30.

The vegetation communities in the Central Delta are characterized by submerged, emergent, floating and riparian communities (Khanna et al., 2011). Submerged aquatic vegetation (SAV) includes native species, such as coontail (*Ceratophyllum demersum L.*), common waterweed (*Elodea canadensis Michx.*), sago pondweed (*Stuckenia pectinata (L.) Boerner*), American pondweed (*Potamogeton nodosus L.*), and non-native plants, such as Brazilian waterweed (*Egeria densa Planch.*), Eurasian watermilfoil (*Myriophyllum spicatum L.*), Carolina fanwort (*Cabomba caroliniana Gray*) and curly-leaf pondweed

(*Potamogeton crispus L.*) (Khanna et al., 2018). The one native species of floating aquatic vegetation (FAV) in the Sacramento–San Joaquin River Delta is pennywort (*Hydrocotyle umbellata L.*) However, after the population crash of pennywort in the early 2000s, the majority of FAV within the central delta are aggressively invasive water hyacinth (*Eichhornia crassipes*) and water primrose (*Ludwigia hexapetala*) (CA State Parks, 2018). The native emergent vegetation found in the Sacramento–San Joaquin River Delta includes tule (*Schoenoplectus spp.*), common reed (*Phragmites australis*) and cattail (*Typha spp*.) (Khanna et al., 2011). Native riparian vegetation species in the Central Delta include willow (*Salix spp.*), live oak (*Quercus spp.*), cottonwood (Populus fremontii), sycamore (*Acer pseudoplatanus*), alder (*Alnus spp.*) and elderberry (*Sambucus spp.*). Invasive riparian species within the Central Delta are giant reed (*Arundo donax L.*), perennial pepperweed (*Lepidium latifolium L.*) and blackberry (*Rubus armeniacus Focke*) (Khanna et al., 2011).

The California Department of Boating and Waterways is the management agency responsible for the abatement of invasive FAV and other weeds in the Sacramento Delta, which is done through the application of chemical herbicides, hand removal, and mechanical removal (Cohen and Carlton, 1995; CA State Parks, 2018). Recreational boating activities generate about half a billion dollars worth of business in Northern California and boating clubs and guide fishing, particularly in the delta region, have been particularly hit the hardest by the effects of invasive FAV. In late fall 2014, invasive FAVs had inundated downtown Stockton and strangled the port to such an extent that it clogged

shipping lanes and forced the city to cancel the 35th annual Delta Reflections Lighted Boat Parade (Hawkes, 2014). Water hyacinth was chemically controlled by California State Park's Division of Boating and Waterways, but the state did not have permission to spray water primrose until 2018 (CA State Parks, 2018). Figure 5 shows the area of interest for this research study occupying areas of very high (red) and high (orange) FAV priority zones.

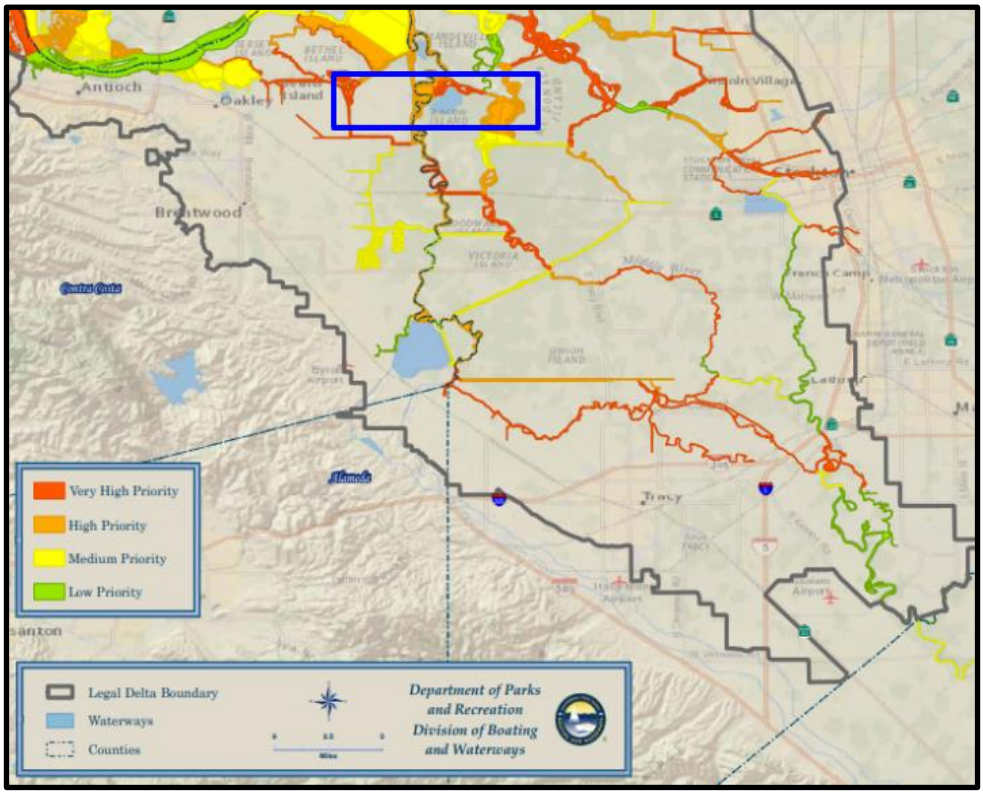

Figure 5. This map shows CA's Division of Boating and Waterways floating aquatic vegetation site prioritization map for 2019. The blue rectangle represents the thesis study AOI (CA State Parks, 2019).

3. Methods & Materials

3.1 Image Classification Methodologies

This research study investigated the most effective remote sensing method of classifying invasive floating aquatic vegetation species by comparing three different types of satellite imagery data: high resolution multispectral 4-band; very high resolution multispectral 8-band; and hyperspectral; as well as four different classification methods: maximum likelihood; spectral vector machine; spectral angle mapper; and object-based imagery analysis. Out of the four classification algorithms, the maximum likelihood is the default algorithm used for most supervised classifications. This classification method has proved effective, regardless of satellite imagery sensor type. Because of this, the ML method was used to compare the accuracy between the three satellite imagery types. The other three methods are unique classification algorithms, one unique classification per satellite imagery type (Table 1). This research study produced six invasive FAV classifications. The accuracy assessments & confusion matrices were produced using ArcGIS Pro.

Table 1. The six algorithms/ imagery combinations investigated throughout this master's thesis.

Classification Algorithm	Spatial Res. / Flight Date	Satellite Sensor	Spectral Info	#of Bands
ML	3.7m - 8/8/2019	PlanetScope	Multispectral	4
SVM	3.7m - 8/8/2019	PlanetScope	Multispectral	4
ML	1.8m - 8/21/2018	WorldView 2	Multispectral	8
OBIA	1.8m - 8/21/2018	WorldView 2	Multispectral	8
ML	2.4m - 8/4/2007	AVIRIS	Hyperspectral	224
SAM	2.4m - 8/4/2007	AVIRIS	Hyperspectral	224

3.2. Invasive FAV Multispectral Classification Analysis (PlanetScope)

In order to classify invasive FAV within the central Sacramento Delta, multispectral satellite imagery from Planet.com was utilized as the 4-band multispectral image option. Planet's multispectral imagery library contains imagery with spatial resolutions between 3.7 m to 1.5 m resolution. Compared to WorldView-2 and AVIRIS imagery, the advantage of using Planet is its up-to-date imagery. Typically, new imagery for a specific area of interest is updated every two to three days. WorldView-2 and AVIRIS imagery are updated once a year to every 5 years depending on the location of the study area. The imaging sensor used was the PlanetScope scene 3.7m resolution sensor, which has the following bands: blue (Band 1, 455–515 nm), green (Band 2, 500–590 nm), red (Band 3, 590–670 nm) and near infrared (Band 4, 780–860 nm). It should be noted that an 8-band version has been announced to be available soon. The multispectral image from Planet was flown on 8/8/2019, has 0% cloud cover, off-nadir angle of 1^{o}, and has a sun elevation angle of 46.4^{o}. The hyperspectral image and the higher-resolution multispectral

images are older images, and both are taken in August as well, that way all six classifications are temporally equally. Since the hyperspectral image has the smallest delta coverage out of the three images, the hyperspectral image's extent was used as the clipping feature for the Planet image (Figure 6).

Figure 6. Clipped extent of PlanetScope 3.7m (8/8/2019) displayed in false-color infrared (4, 3, 2).

3.2.1 Training & Validation Fieldwork for Planet Imagery

The Planet imagery was flown on Thursday, August 8th, 2019. Training area samples and accuracy assessment samples for the Planet imagery analysis were collected on Friday, August 9th, 2019 from 8:30 am - 11:30 am. In order to access the delta island groups, a motorboat was rented from Sugar Barge Marina Bethel Island, CA (38.026693, -121.612340). A Trimble Juno GPS receiver was used to acquire training and validations points. The original plan was to position the boat as close to the FAVs to select training and validations points on top. After consulting the boat rental employees, it was advised to keep a safe distance (>10ft) from FAVs at all costs in order to avoid the plants. FAV has a tendency of wrapping around boat propellers as well as getting the FAVs stuck in the

engine intake. If the invasive FAV are broken up by boating activities, the broken piece can drift downstream and form new FAV colonies.

A total of 400 points were acquired; 200 training samples and 200 accuracy assessment points. 80 training samples of FAV (both water primrose and water hyacinth); 40 native vegetation training samples; 40 water training samples; 40 bare soil training samples; 110 FAV accuracy assessment points; 30 native vegetation accuracy assessment points, 30 water accuracy assessment points; 30 bare soil accuracy assessment points. These 400 points were used for both the SVM and ML Planet classifications.

3.2.2 ML & SVM PlanetScope Preprocessing

Before the classifications begin, a 14.39 km^2 mask of inner delta islands (Figure 6) was used to raster clip the Planet image, which allowed only vegetation within the delta channels and not agricultural fields to be classified. The clipping boundary between the delta and land are the levee roads, in order to ensure that any invasive FAV along the levee walls can be identified. Inner delta islands such as Little Mandeville and Mildred islands are not excluded from the classification.

3.2.3 Maximum Likelihood Classification

The maximum likelihood classification was run on the clipped PlanetScope image using 3 out of 4 available bands: 4 (infrared); 3 (red); 2 (green). This classification method is the control classifier to test variability between the three satellite images. This classification method is performed using Erdas Imagine remote sensing software using default parameters. The Planet image training samples and accuracy assessment points

were chosen based on ground-truthed GPS from fieldwork. The Planet ML accuracy assessment and confusion matrix were post-processed using ArcGIS Pro.

3.2.4 Support Vector Machine Classification

The SVM classification was run on the clipped PlanetScope image using the false-color infrared band combination: RBG 4,3,2. The advantage of the SVM method compared to the other four algorithms its ability to successfully handle small training data sets, often producing higher classification accuracies than the traditional methods (Mantero et al., 2005). The SVM classification used the same 200 training samples as the maximum likelihood. This classification method was performed using ENVI remote sensing software. The classification parameter of 800 maximum pixels per classification class was used. The value of 800 was chosen because it produced the best SVM classification results. The Planet SVM accuracy assessment and confusion matrix were post-processed using ArcGIS Pro. For the Planet SVM classification, the same 200 ML ground-truthed validation points were used.

3.3 Invasive FAV Multispectral Classification Analysis (WorldView-2)

The second type of satellite imagery being used to classify invasive FAV is high-resolution multispectral imagery from WorldView-2 (WV2) satellite. Compared to the Planet and AVIRIS imagery, the advantage of using WorldView-2 imagery is its high spatial resolution and its eight multispectral bands. This satellite sensor has a spatial resolution of 1.8m and has eight multispectral bands: coastal (band 1, 400-450 nm), blue (band 2, 450-510 nm), green (band 3, 510-580 nm), yellow (band 4, 585-625 nm), red (band 5, 630-690 nm), red edge (band 6, 705-745 nm), near-infrared 1 (band 7, 770-895

nm), near-infrared 2 (860-1040 nm). The image was flown on August 21st, 2018; cloud cover of 0%; off-nadir 18.9°; and sun elevation of 60.42°. Before segmentation and classification, a 14.39 km^2 mask of inner delta islands (Figure 7) was used to raster clip the WorldView-2 image, which allowed only wetland vegetation and not agricultural fields to be classified.

Figure 7. Clipped extent of WorldView-2 1.8m (8/21/2018) displayed in false-color infrared (8, 5, 3).

3.3.1 WorldView-2 Maximum Likelihood Classification

The maximum likelihood classification was run on the clipped WorldView-2 image using the false-color infrared band subset: 8 (near-infrared 2); 5 (red); 3 (green). The WorldView-2 ML classification method was performed using Erdas Imagine remote sensing software. 200 new training samples and 200 new validation points are used. These are not the same points as the Planet imagery, since WV2 is older imagery, these points were acquired based on the imagery itself (Figure 8), not through GPS fieldwork. The WV2 maximum likelihood classification used 200 training samples: 80 training samples of invasive FAV; 40 native vegetation training samples; 40 water training samples; 40 bare soil training samples. The WorldView-2 ML accuracy assessment and confusion matrix

table were processed using ArcGIS Pro using 200 validation points: 110 invasive FAV points; 30 native vegetation points; 30 water points; and 30 bare soil points.

Figure 8. This snapshot from the WorldView-2 image flown on 8/21/2018 shows the distinct spectral differences between the bright green invasive FAV floating mats, the surrounding delta water, and the darker green native vegetation.

3.3.2 WorldView-2 Object-Based Imagery Analysis

The OBIA classification method was performed using eCognition remote sensing software with the WV2 image displayed in false color infrared band subset: 8 (near infrared 2); 5 (red); 3 (green). The multiresolution segmentation used a scale parameter of 20, as well as a shape value of 0.2 and a compactness value of 0.5. The scale parameter of 20 allowed for smaller clumps of invasive FAV to be segmented, a larger scale parameter wouldn't separate the FAV from native vegetation, but instead, the smaller FAV segments would be grouped into the native vegetation segments. A higher color value of 0.2 resulted in the most accurate segmentation, instead of the default 0.1. After segmentation, training areas were assigned to the newly segmented polygons. The imagery is from 8/21/2018 and

therefore training segment polygons and accuracy assessment points were acquired based on the imagery itself, not from GPS fieldwork (see Figure 8). Keeping the proportions used in the previously described methods and imagery, 200 training segment polygons: 80 training polygons of invasive FAV; 40 native vegetation training polygons; 40 water training polygons; 40 bare soil training polygons. The nearest-neighbor algorithm was used to classify during the OBIA. The WorldView-2 OBIA accuracy assessment and confusion matrix table were processed using ArcGIS Pro using 200 validation points: 110 invasive FAV points; 30 native vegetation points; 30 water points; and 30 bare soil points.

3.4 Invasive FAV Hyperspectral Analysis (AVIRIS)

Airborne remotely sensed hyperspectral imagery for the Central Sacramento-San Joaquin Delta Region was acquired using the Airborne Visible/Infrared Imaging Spectrometer (AVIRIS) sensor by the Jet Propulsion Laboratory (JPL, Pasadena, California, USA). This hyperspectral sensor does not have a fixed altitude like a satellite, but instead, this sensor is flown using a plane. This means that the spatial resolution for AVIRIS depends on the flight altitude. For this imagery, the flight elevation resulted in a spatial resolution of 2.4m. The AVIRIS image was flown on 8/4/2007 from east to west and has a solar elevation of 66.56^{o}. The AVIRIS image has the smallest spatial coverage out of the three remote sensing images, the hyperspectral is used as the 14.39 km^2 study area extent for the 6 invasive FAV classifications (Figure 9). Because this image is from 12 years ago and is not current, the training samples and regions of interest (ROI) were acquired based on the imagery itself.

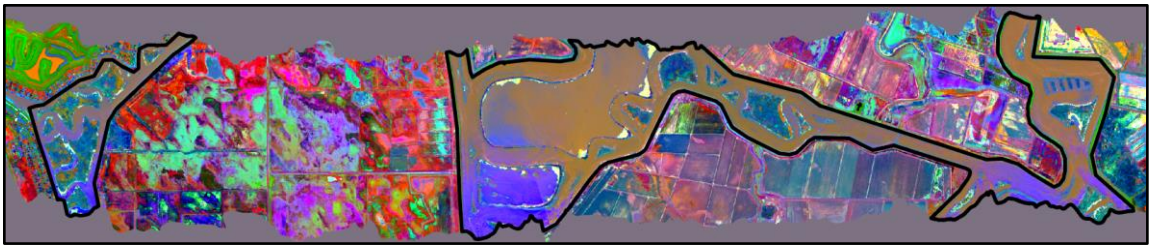

Figure 9. Clipped extent of AVIRIS hyperspectral 2.4m (8/4/2007) displayed in band combination (11, 9, 7) which is from a MNF 100 band subset, reduced from 224 bands.

The advantage of using AVIRIS hyperspectral imagery, compared to multispectral WorldView-2 (8-bands) and Planet imagery (4-bands), is its amount of spectral bands, its narrowness of spectral bands, and its spatial resolution. Hyperspectral imaging systems have made it possible for the collection of several hundred spectral bands in a single acquisition, thus producing many more detailed spectral data (Govender et al., 2007; Kokaly et al., 2003). AVIRIS has a spectral range from 360 - 2500 nm with a total of 224 bands. The higher number of bands creates a greater potential for identifying the specific wavelengths that correspond with the reflectance of invasive FAV. However, with the advances in hyperspectral technologies, practical issues related to increased image resolution, data volumes, and data-processing costs and times, are considered. Hyperspectral imagery may be expensive and hard to acquire; however, NASA's JPL operates the AVIRIS sensor and offers a free data portal of previously flown hyperspectral data.

3.4.1 Spectral Angle Mapper Classification Analysis

The SAM invasive FAV classification was performed using ENVI hyperspectral imagery software and the classification workflow tool. The first reduction of

dimensionality was performed by manually selecting good bands from bad bands. A bad band contains no spectral information - which is caused by sensor malfunction - or contains static noise. The manual reduction resulted in 206 out of 224 bands as good bands. The second reduction of dimensionality used the Minimum Noise Fraction (MNF), reducing the 206 spectral bands to a 100-band subset. Out of the 100 MNF bands, the MNF band subset of 11, 9, 7 resulted in the best contrast display between invasive FAV and native vegetation (see Figure 9). ROIs were acquired using this band display. The 100 MNF subset was reduced a second time by selecting clean vs noisy bands, resulting in a 20-good band MNF subset. The spectral angle mapper algorithm was performed using the 20-band subset with an angle of 1.57 radians. This specific angle was determined through trial and error. The ROI tool was used to create reflectance signatures for the classification categories based on the AVIRIS image itself (Figure 10): 80 ROIs samples of invasive FAV; 40 ROIs of native vegetation; 40 ROIs of delta water; and 40 ROIs of levee / bare soil. Each ROI sample is 4 (2.4m^2) pixels. The reflectance values for the four classification categories are displayed graphically in Figure 11. ArcGIS Pro was used to produce the accuracy assessment and confusion matrix table for the SAM classification. 200 validation points were displayed on top of the AVIRIS SAM layer: 30 native vegetation; 110 invasive FAV; 30 delta water; 30 levee / bare soil.

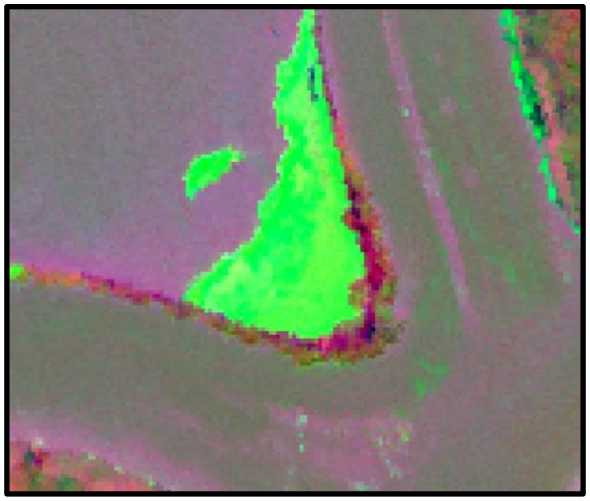

Figure 10. This snapshot from the AVIRIS Hyperspectral 2.4m (8/4/2007) displays the distinct spectral difference between the bright green invasive FAV floating mats and the surrounding delta water and native vegetation. Due to this distinction, accurate training and validation sites were chosen based on the imagery itself.

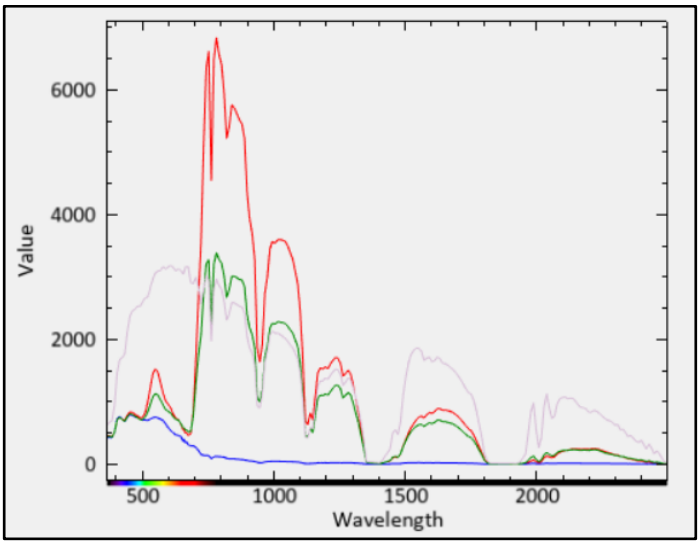

Figure 11. This graph displays the reflectance values of the four ROI classes used for the SAM and ML hyperspectral classifications. Invasive FAV: red, native vegetation: green, bare soil: gray, water: blue.

3.4.2 Maximum Likelihood Classification

The maximum likelihood classification for the AVIRIS hyperspectral image was classified using ENVI remote sensing software. The classification workflow tool was used

to conduct the maximum likelihood classification. The AVIRIS ML classification used a MNF three band subset of (11, 9, 7). The same SAM ROIs were used to produce the invasive FAV AVIRIS maximum likelihood classification: 80 ROIs samples of invasive FAV; 40 ROIs of native vegetation; 40 ROIs of delta water; and 40 ROIs of levee / bare soil. Same as the AVIRIS spectral angle mapper, 200 validation points were displayed on top of the AVIRIS maximum likelihood layer using ArcGIS Pro: 30 Native Veg; 110 FAV; 30 Water; 30 Bare Soil.

4. Results

4.1 Multispectral Planet Classifications

The results of the PlanetScope invasive FAV maximum likelihood and support vector machine classifications are displayed below in full extent (Figure 12) The invasive FAV are represented by the red polygons, the native delta vegetation are represented by green polygons, the delta water is represented by blue polygons, and the levee roads / bare soils are represented by gray polygons. The ML confusion matrix results are displayed in (Table 4) and the SVM confusion matrix results are displayed in (Table 5).

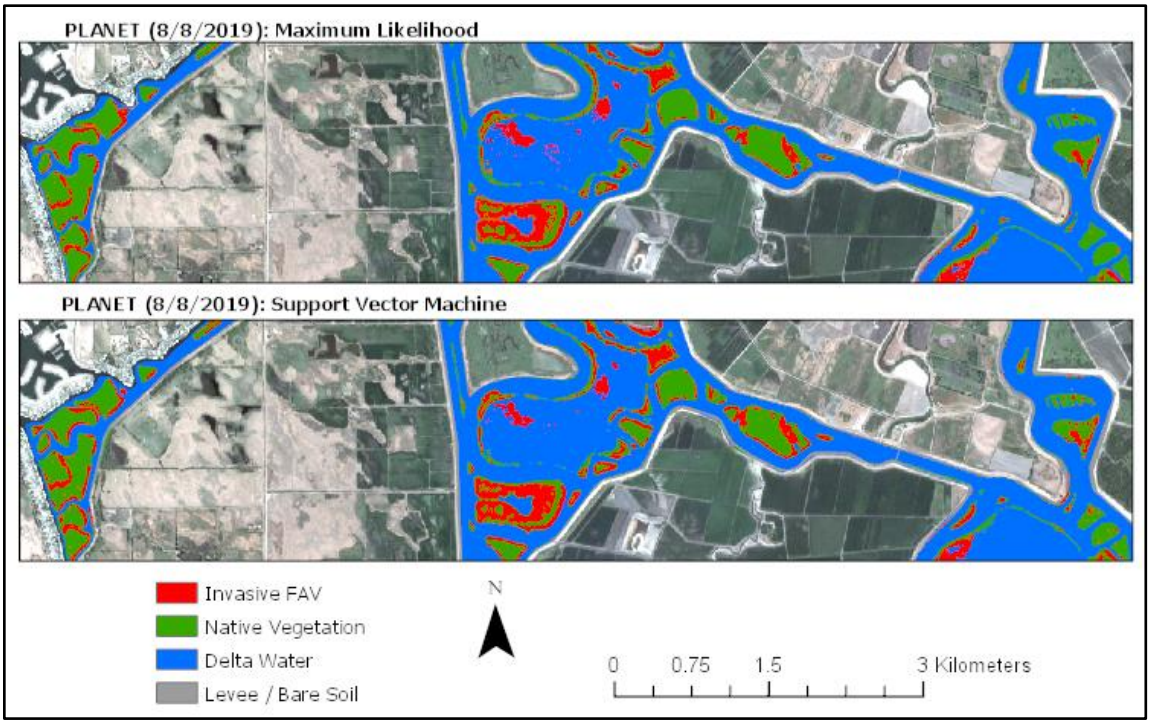

Figure 12. Full extent of PlanetScope 3.7m (8/8/2019) ML & SVM Classifications.

The Planet multispectral (3.7m) resolution maximum likelihood invasive FAV classification resulted in a producer accuracy of 0.85 and a user accuracy of 0.99, and an overall accuracy of 0.91 (Table 4). Classification errors were along the boundary between the islands and the delta water. This classification method resulted in a thin polygon of native vegetation between the invasive FAV and delta water. This is most noticeable in the Sandmound Slough Islands (Figure 13) sub-study site along the rims of the islands within the slough. The classification errors were likely caused by the reflectance signature of the water / island boundary being similar to the reflectance of the native vegetation. The Planet imagery does not sufficiently create a well-defined boundary between the vegetation and water, which is caused by the coarse resolution of the image. Therefore, displaying a drastic color gradient which creates a likely source for error.

Table 4. Planet (8/8/2019) Maximum Likelihood Classification Confusion Matrix

ClassValue	NativeVeg	FAV	Water	BareSoil	Total	U_Accuracy	Kappa
NativeVeg	29	15	0	0	44	0.66	0
FAV	1	94	0	0	95	0.99	0
Water	0	1	30	0	31	0.97	0
BareSoil	0	0	0	30	30	1	0
Total	30	110	30	30	200	0	0
P_Accuracy	0.97	0.85	1	1	0	0.91	0
Kappa	0	0	0	0	0	0	0.87

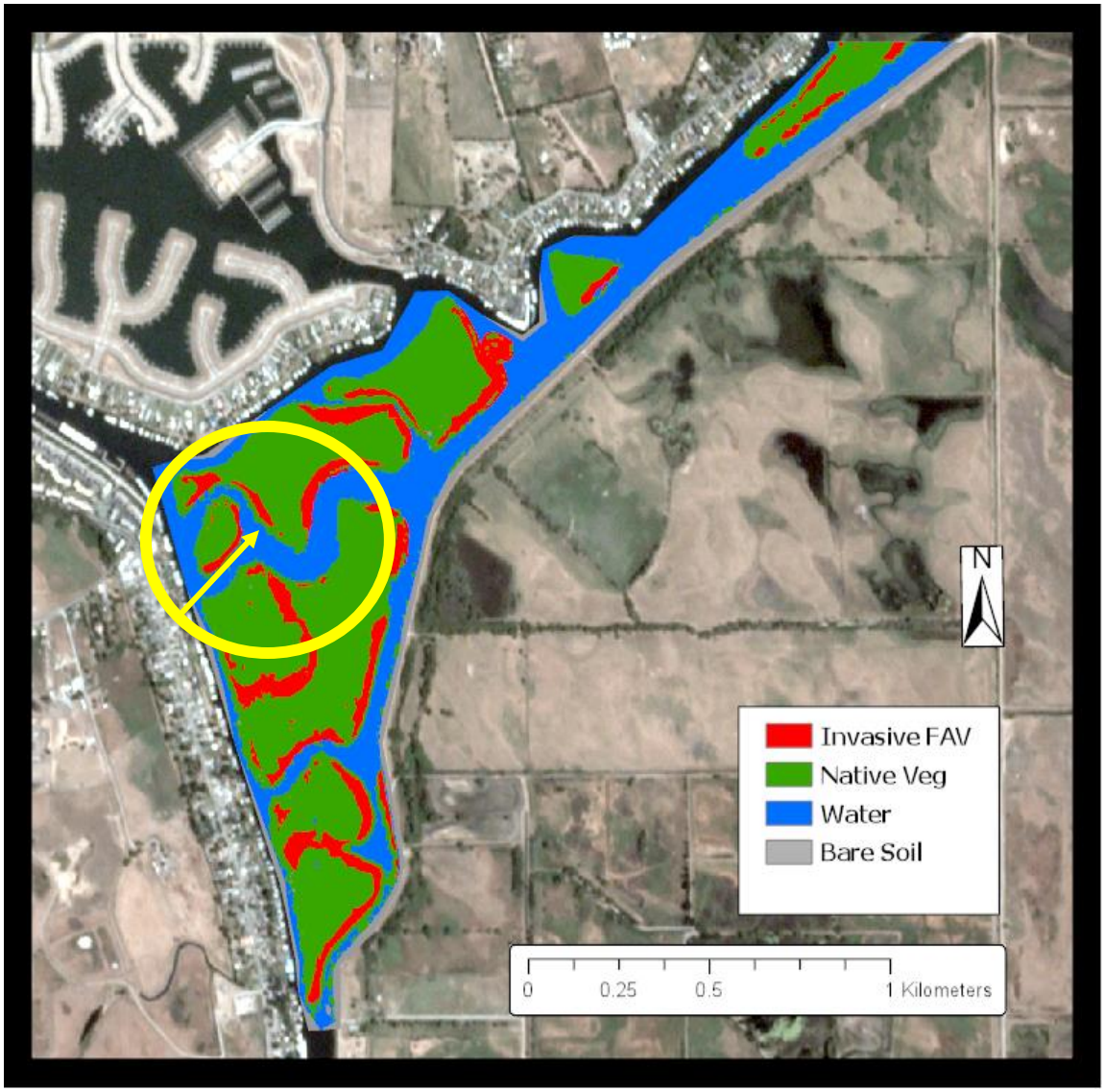

Figure 13. Planet (8/8/2019) Maximum Likelihood Invasive FAV Classification: Sandmound Slough Islands study site. The area within the yellow ellipse highlights the misclassification of the boundary between the water and the invasive FAV, classifying this boundary as a thin strip of native vegetation between the FAV and water.

The PlanetScope multispectral (3.7m) resolution support vector machine invasive FAV classification resulted in a producer accuracy of 0.83, a user accuracy of 0.99, and an overall accuracy of 0.9 (Table 5). Like the Planet maximum likelihood, the SVM classification resulted in errors mainly along the boundary between the islands and the delta water. This classification method resulted in a thin polygon of native vegetation between the invasive FAV and delta water. This is evident in each of the three-study area sub-groups; however it is most noticeable in Sandmound Slough Islands (Figure 14) sub-study area. The Planet support vector machine classification error was likely caused by the reflectance signature of the water / island boundary being similar to the reflectance of the native vegetation. The strength of the SVM classifier is its ability to have success with an unevenly distributed amount of training samples. To fix the SVM classification errors, more training samples of invasive FAV and less training samples of native vegetation, water, and bare soil might help reduce misclassification.

Table 5. Planet (8/8/2019) Support Vector Machine Classification Confusion Matrix

ClassValue	Native Veg	FAV	Water	Bare Soil	Total	U_Accuracy	Kappa
Native Veg	29	19	0	0	48	0.61	0
FAV	1	91	0	0	92	0.99	0
Water	0	0	30	0	30	1	0
Bare Soil	0	0	0	30	30	1	0
Total	30	110	30	30	200	0	0
P_Accuracy	0.97	0.83	1	1	0	0.9	0
Kappa	0	0	0	0	0	0	0.85

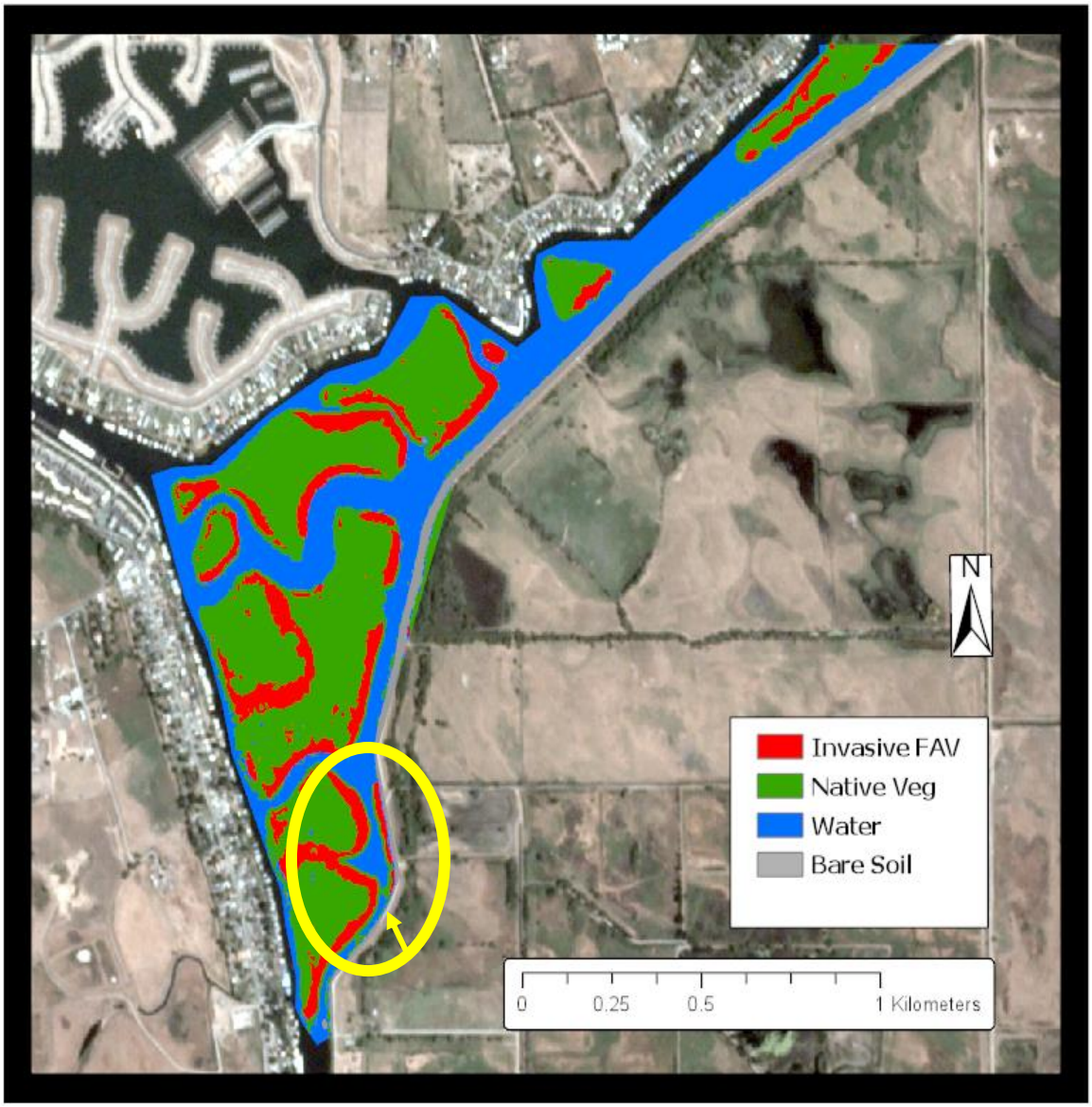

Figure 14. Planet (8/8/2019) Support Vector Machine Invasive FAV Classification: Sandmound Slough Islands study site. The area within the yellow ellipse highlights the misclassification of the boundary between water and invasive FAV, incorrectly classifying this boundary as a thin strip of native vegetation between the FAV and water.

4.2 Multispectral WorldView-2 Classifications

The results of the WorldView-2 invasive FAV maximum likelihood and object-based image analysis classifications are displayed below in full extent (Figure 15) The invasive FAV are represented by the red polygons, the native delta vegetation are represented by green polygons, the delta water is represented by blue polygons, and the levee roads / bare soil are represented by gray polygons. The ML confusion matrix results are displayed in Table 6 and the OBIA confusion matrix results are displayed in Table 7.

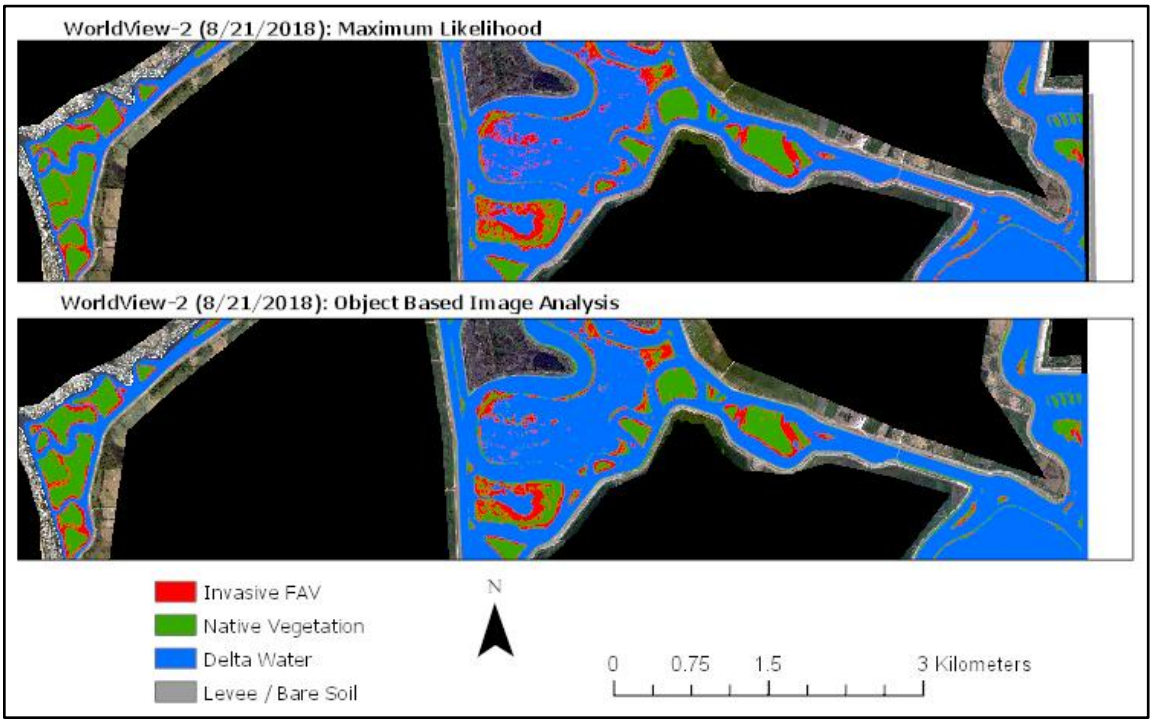

Figure 15. Full extent of WorldView-2 1.8m (8/21/2018) ML & OBIA Invasive FAV classifications.

The WorldView-2 multispectral high resolution (1.8m) maximum likelihood invasive FAV classification resulted in a producer accuracy of 0.90, a user accuracy of 0.94, and an overall accuracy of 0.91 (Table 6). The classification errors that occurred during this ML classification were mainly the misclassification of invasive FAV as native vegetation. The two horseshoe shaped islands in the Little Mandeville Island (Figure 16) sub-group had the most intense misclassification of invasive FAV as native vegetation. In these islands, the invasive FAV clogs the entire inside of the inundated levee islands, creating an island filled with invasive FAV with a horseshoe shaped native vegetation outer boundary. This error was likely caused by the reflectance value of the invasive FAV towards the interior of the horseshoe islands being too similar to the reflectance value of the native vegetation, which created patches of classified native vegetation in the middle of the horseshoe. To try and eliminate sources of error, more training samples of both invasive FAV and native vegetation would need to be acquired.

Table 6. WorldView-2 (8/21/2018) Maximum Likelihood Classification Confusion Matrix

ClassValue	NativeVeg	FAV	Water	BareSoil	Total	U_Accuracy	Kappa
NativeVeg	28	11	4	0	39	0.71	0
FAV	2	99	0	0	105	0.94	0
Water	0	0	26	0	26	1	0
BareSoil	0	0	0	30	30	1	0
Total	30	110	30	30	200	0	0
P_Accuracy	0.93	0.90	0.87	1	0	0.91	0
Kappa	0	0	0	0	0	0	0.87

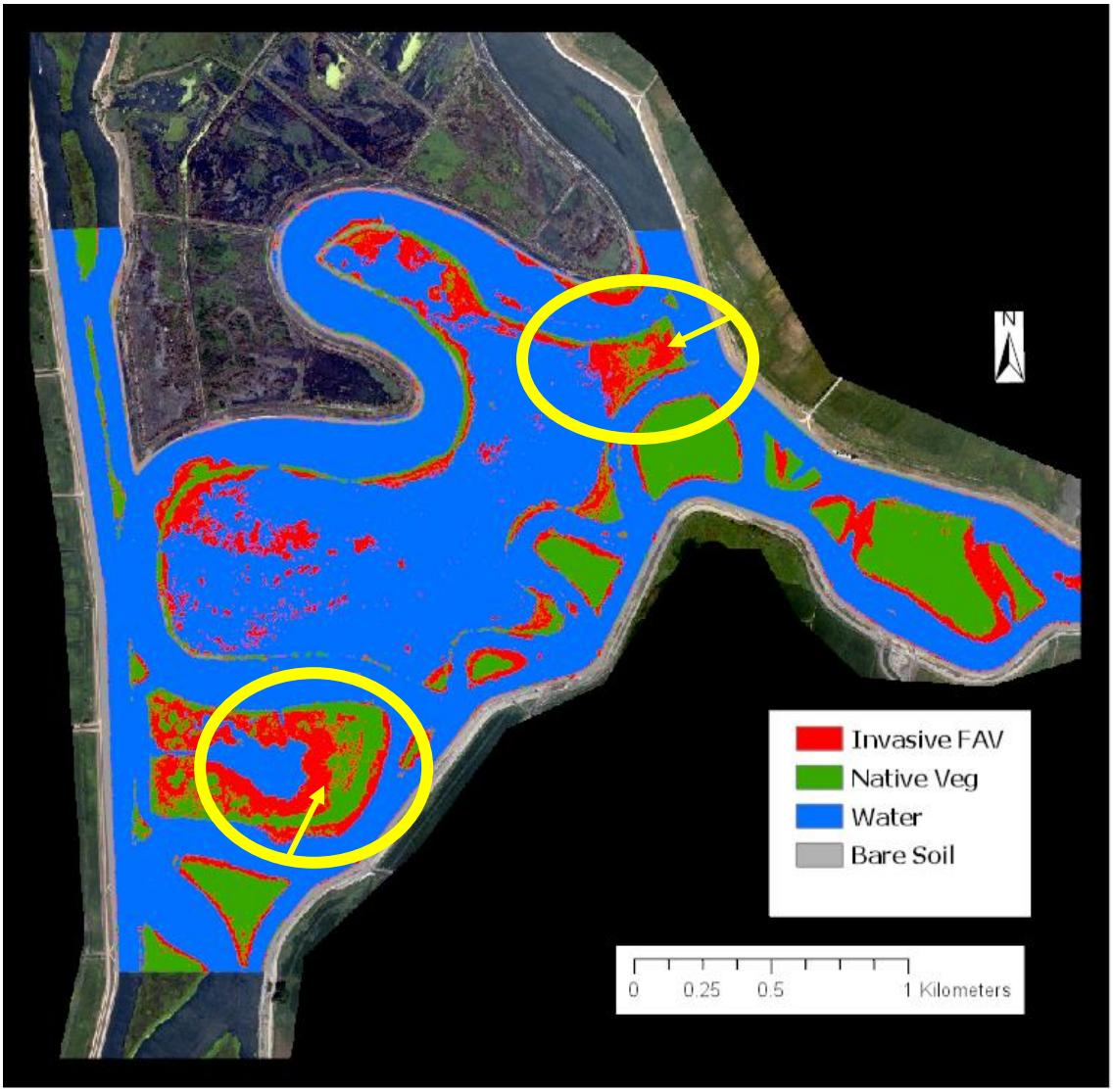

Figure 16. WorldView-2 (8/21/2018) Maximum Likelihood Invasive FAV Classification: Little Mandeville Islands study site. This sub-study site contains many horseshoe-shaped inundated levee islands, these islands are perfectly shaped to trap invasive FAV mats. The areas within the yellow ellipses show the misclassification of native vegetation inside the horseshoe islands where there is only invasive FAV.

The WorldView-2 multispectral high resolution (1.8m) OBIA invasive FAV classification resulted in a producer accuracy of 0.86 and a user accuracy of 0.97, and an overall accuracy of 0.89 (Table 7). The classification error that occurred during the OBIA classification were mainly the misclassification of smaller FAV mats as small islands of native vegetation. The OBIA classified some of these small invasive FAV mats as tiny islands of native vegetation, instead of invasive FAV. It is most noticeable in the Little Mandeville Island (Figure 17) sub-group in the center of the study area. When this imagery was flown in August 2018, there was a large presence of small invasive FAV mats floating in the open delta water that had broken off of the upper inundated levee island. This error was likely caused by the reflectance value of the smaller invasive FAV being too similar to the reflectance value of the native vegetation. In order to fix this misclassification, more native vegetation training samples would need to be acquired.

Table 7. WorldView-2 (8/21/2018) OBIA Classification Confusion Matrix

ClassValue	Native Veg	FAV	Water	Bare Soil	Total	U_Accuracy	Kappa
Native Veg	27	15	3	0	45	0.60	0
FAV	3	95	0	0	98	0.97	0
Water	0	0	27	0	327	1	0
Bare Soil	0	0	0	30	30	1	0
Total	30	110	30	30	200	0	0
P_Accuracy	0.90	0.86	0.90	1	0	0.89	0
Kappa	0	0	0	0	0	0	0.84

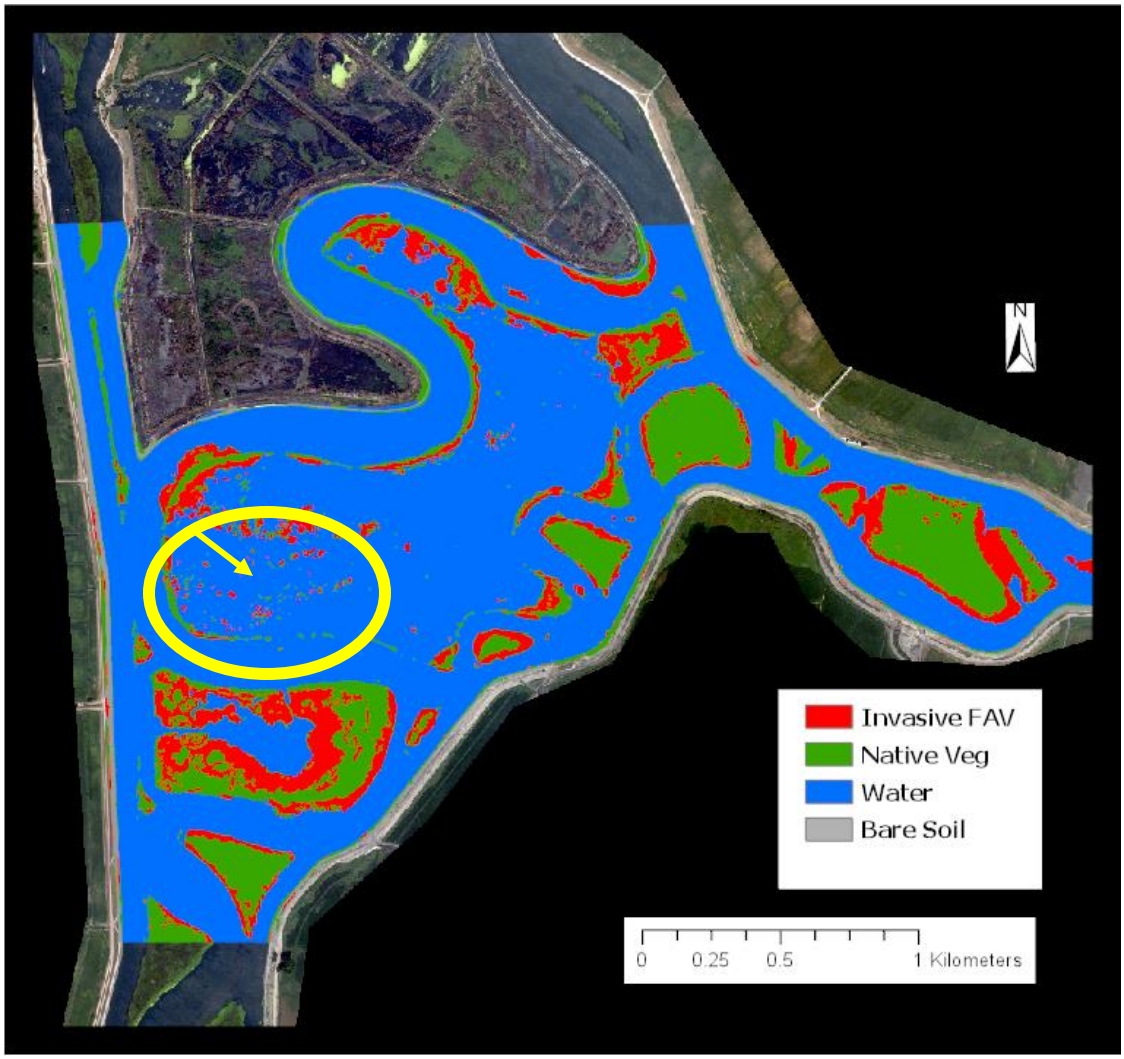

Figure 17. WorldView-2 (8/21/2018) OBIA Invasive FAV Classification: Little Mandeville Islands study site. The main error resulting from the OBIA classification were the misclassification of smaller FAV mats as small islands of native vegetation. These misclassified small FAV mats are highlighted by the yellow ellipse.

4.3 Hyperspectral AVIRIS Classifications

The results of the AVIRIS hyperspectral invasive FAV maximum likelihood and spectral angle mapper classifications are displayed below in full extent (Figure 18). The invasive FAV are represented by the red polygons, the native delta vegetation are represented by green polygons, the delta water are represented by blue polygons, and the levee roads / bare soil are represented by gray polygons. The ML confusion matrix results are displayed in Table 8 and the SAM confusion matrix results are displayed in Table 9.

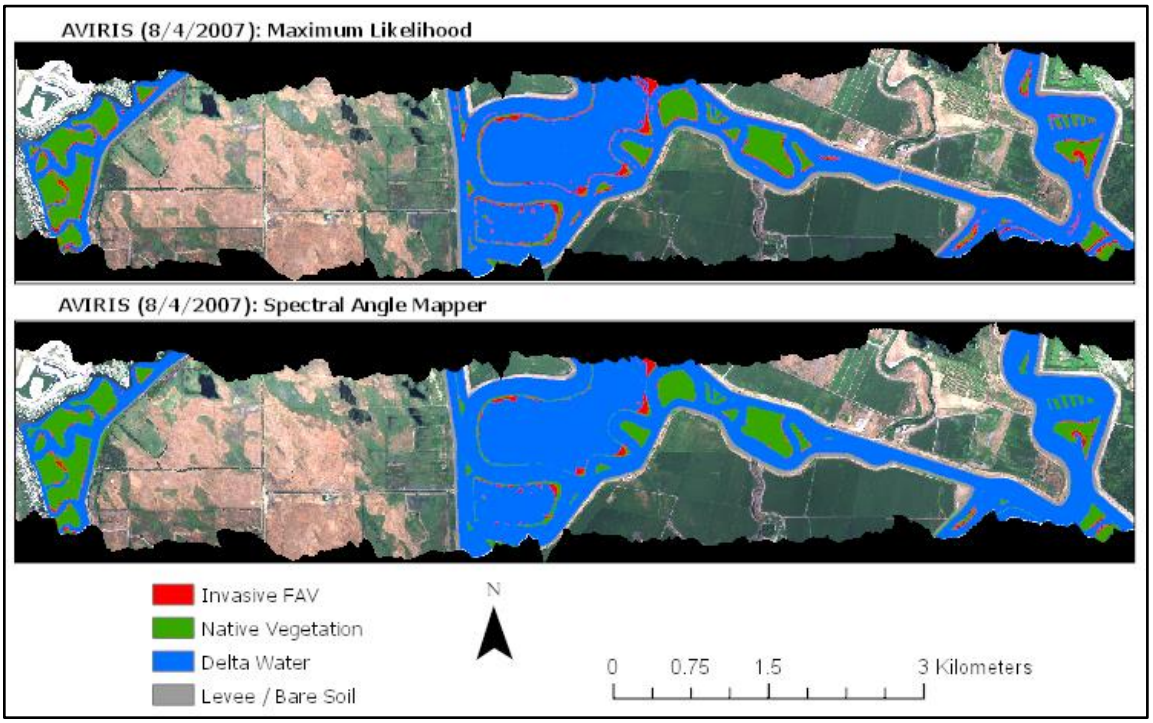

Figure 18. Full extent of AVIRIS Hyperspectral 2.4m (8/4/2007) ML & SAM Invasive FAV classifications.

The AVIRIS hyperspectral maximum likelihood invasive FAV classification resulted in a producer accuracy of 0.87, a user accuracy of 0.86, and an overall accuracy of 0.85 (Table 8). The AVIRIS hyperspectral maximum likelihood classification errors were mainly along the boundaries between the islands and the delta water, classifying invasive FAV in areas where there was no FAV present. This is evident in each of the three-study area sub-groups but most noticeable in the Upper Mildred Island sub-group (Figure 19). The upper levee island has a large over-classification of invasive FAV along the entire rim of the inundated levee, but in reality, the invasive FAV is not as constant as represented by the classified image. The FAV classification error is likely caused by the reflectance signature of the water / island boundary. In order to fix this misclassification, more training samples of both invasive FAV and native vegetation would need to be acquired.

Table 8. AVIRIS Hyperspectral (8/4/2007) Maximum Likelihood Confusion Matrix

ClassValue	Native Veg	FAV	Water	Bare Soil	Total	U_Accuracy	Kappa
Native Veg	25	12	1	0	38	0.66	0
FAV	5	96	10	0	111	0.86	0
Water	0	2	19	0	21	0.90	0
Bare Soil	0	0	0	30	30	1	0
Total	30	110	30	30	200	0	0
P_Accuracy	0.83	0.87	0.63	1	0	0.85	0
Kappa	0	0	0	0	0	0	0.76

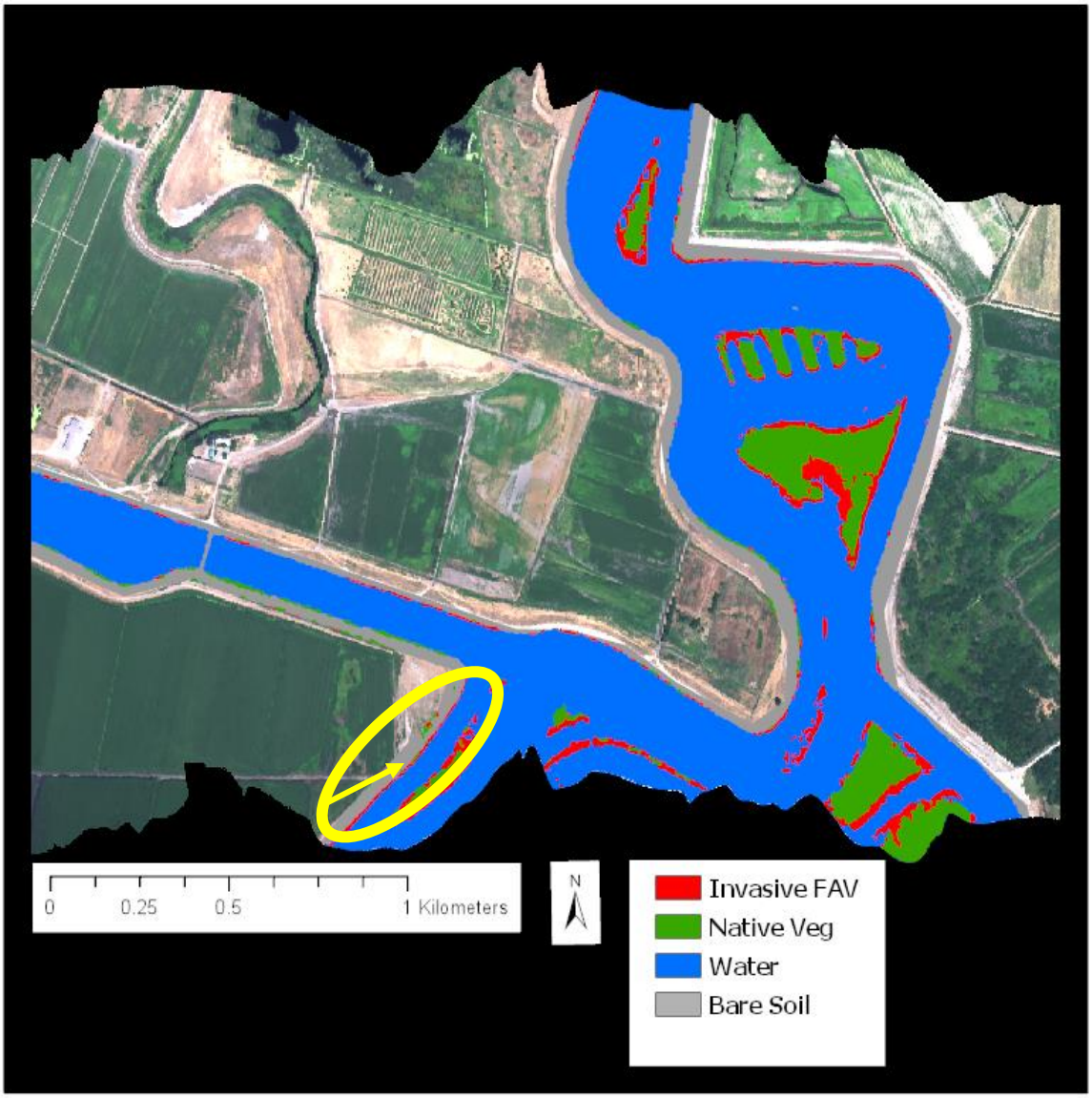

Figure 19. AVIRIS Hyperspectral (8/4/2007) Maximum Likelihood Invasive FAV Classification: Upper Mildred Islands study site. The yellow ellipse highlights an area of misclassified invasive FAV along levee roads.

The AVIRIS hyperspectral spectral angle mapper invasive FAV classification resulted in a producer accuracy of 0.91, a user accuracy of 0.90, and an overall accuracy of 0.89 (Table 9). In the central delta research study area, AVIRIS SAM classification resulted in the highest invasive FAV producer accuracy. Similar to the AVIRIS maximum likelihood classification, the spectral angle mapper also resulted in errors of over classifying invasive FAV, but not as many as the AVIRIS ML. Instead of a thin strip of invasive FAV along the levee roads, small patches of invasive FAV were classified inside large delta islands, areas where there would only be native vegetation present. The invasive FAV would only be present on the outer perimeter of the islands, being that they are floating mats of aquatic vegetation. An example of these classification errors can be seen on the levee roads on the left side of the Upper Mildred Island sub-group (Figure 20). These errors were likely caused by the SAM's endmember collection process. SAM compares the angle between the endmember spectrum vector and each pixel vector. If the AVIRIS sensor was flown at a lower altitude creating a finer spatial resolution, this might allow for a better endmember angle comparison, resulting in a more accurate classification.

Table 9. AVIRIS Hyperspectral (8/4/2007): Spectral Angle Mapper Confusion Matrix

ClassValue	Native Veg	FAV	Water	Bare Soil	Total	U_Accuracy	Kappa
Native Veg	25	9	0	0	34	0.73	0
FAV	5	101	6	0	112	0.90	0
Water	0	0	24	1	25	0.96	0
Bare Soil	0	0	0	29	329	1	0
Total	30	110	30	30	200	0	0
P_Accuracy	0.83	0.91	0.80	0.96	0	0.89	0
Kappa	0	0	0	0	0	0	0.83

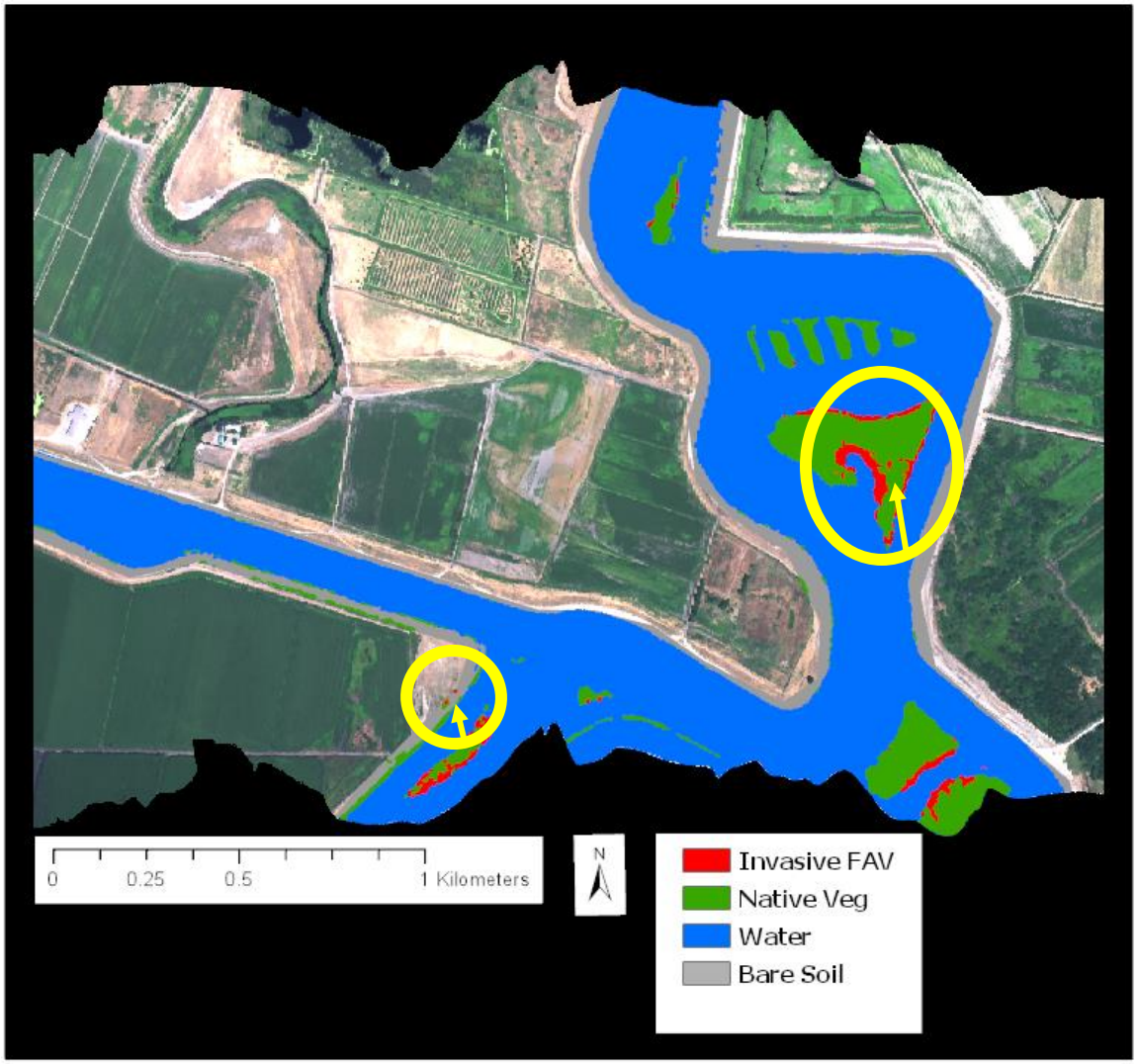

Figure 20. AVIRIS Hyperspectral (8/4/2007): Spectral Angle Mapper Invasive FAV Classification: Upper Mildred Islands study site. These yellow ellipses highlight the misclassifications of invasive FAV as small patches along the levee roads as well as within the Upper Mildred islands. These small patches of misclassified FAV are really patches native vegetation.

4.4 Accuracy Assessment Results

In order to equally compare the invasive FAV accuracy assessments, all six classifications used the same number of accuracy assessments points: 30 native vegetation; 110 invasive FAV; 30 delta water; 30 levee / bare soil. All validation points were chosen based on the reference images (AVIRIS, WorldView-2) or fieldwork (Planet) and then compared with their location on the resulting classification layers. Since each image was flown during a different year (2007, 2018, 2019), the 200 validation points were selected from different locations within the study area, depending on the imagery used. In addition to the differing flight dates, the invasive FAV mats are not stationary. FAV mats slowly drift through the delta channels. Even though each image was flown during a different year, each image was flown during the same time of year: August. August is the blooming stage for invasive hyacinth and invasive primrose, making it the most logical time of the year to classify with aerial imagery. If the time of year is the same for the Planet, WorldView-2, and AVIRIS images, a comparison of accuracies can be effectively analyzed regardless of the differing years.

The accuracy assessments were reported using confusion matrix tables (see Tables 4-9), displaying three accuracy assessment values: overall accuracy; user's accuracy; and producer's accuracy. This research study is only interested in the comparisons between the invasive FAV class accuracy values, not native vegetation, water, or bare soil. In addition, this research study is not interested in comparing the area of invasive FAV identified during each of the six classifications. Since the three remote sensing images were all flown during

different years, the amount of invasive FAV present in each image is different. Because of this difference, only accuracy assessment values were compared.

The overall accuracy value represents, out of all of the reference sites, what proportion is mapped correctly. The overall accuracy value is calculated by the number of correctly classified sites divided by the total number of reference sites (Table 10).

The user's accuracy (U_Accuracy) is the accuracy from the point of view of a map user, not the map maker. The user's accuracy represents how often the class on the map will be present on the ground (Table 10). The user's accuracy is a complement of the "Error of Commission". If the validation points were acquired from the classified rasters, and then compared to their location on the reference image (satellite image), then the user's accuracy value would produce the most reliable accuracy assessment value. The validation points for this research study were chosen based on the reference image, not the classified image.

The accuracy of identifying invasive FAV is represented by the producer's accuracy (P_Accuracy) value. Producer's accuracy is the classified map accuracy from the point of view of the map maker (the producer). This accuracy value represents how often real features on the ground are correctly shown on the classified map, or the probability that a certain land cover of an area on the ground is classified as such (Table 10). The producer's accuracy is a complement of the "Error of Omission." Since the accuracy assessment points for this research study were acquired from the reference image and then compared with their location on the classified image, the producer's accuracy value is the accuracy value that best reflects the overall effectiveness of classifying invasive FAV.

The different classification method / imagery combination results in a range of invasive FAV producer's accuracy values between 83% - 91% (Table 10). Comparing the three maximum likelihood classifications: the PlanetScope maximum likelihood classification resulted in an invasive FAV accuracy value of 85%; the AVIRIS hyperspectral maximum likelihood classification resulted in an invasive FAV accuracy of 87%; and the WorldView-2 multispectral maximum likelihood resulted in an invasive FAV accuracy of 90%.

Comparing the three unique classification algorithms: the AVIRIS hyperspectral spectral angle mapper classification resulted in an invasive FAV accuracy of 91%, the highest producer accuracy percentage of the six invasive FAV classifications; the WorldView-2 multispectral object-based image analysis resulted in an invasive FAV accuracy of 86%; the PlanetScope multispectral support vector machine classification of the Planet multispectral imagery resulted in an invasive accuracy of 83%, the lowest producer accuracy percentage of the six invasive FAV classifications.

Table 10. The six algorithms/imagery combinations and their resulting FAV producer's accuracies, FAV user's accuracies, and overall accuracies.

Algorithm/Imagery Combination	Invasive FAV Producer's Accuracy Value	Invasive FAV User's Accuracy Value	Overall Accuracy
Planet (ML)	0.85	0.99	0.91
Planet (SVM)	0.83	0.99	0.90
WorldView-2 (ML)	0.90	0.94	0.91
WorldView-2 (OBIA)	0.86	0.97	0.89
AVIRIS (ML)	0.87	0.86	0.85
AVIRIS (SAM)	0.91	0.90	0.89

5. Discussion

Out of the six classification/imagery combinations, the spectral angle mapper classification of the AVIRIS hyperspectral image from 8/4/2007 rendered the highest producer accuracy for identifying invasive FAV. The PlanetScope support vector machine classification delivered the lowest producer accuracy for identifying invasive FAV.

Even though the results from this research study revealed the spectral angle mapper algorithm as the most effective classification option, the three other classifiers are very effective as well. All six invasive FAV producer accuracy percentages range from 83% - 91%. Ideally, the six classifications should have used the ground-truthed GPS training and validation points. Unfortunately, since each image is from a different year, the training and validation points are different for each of the three aerial images, due to the drifting nature of water hyacinth and water primrose.

For this research study, the ML classifier was used as the control method, allowing for a comparison between the three different satellite imagery types. In this specific study, the maximum likelihood produced the 2nd (WV2), 3rd (AVIRIS), and 5th (Planet) producer accuracies for invasive FAV classifications. The results of the ML comparison show that, regardless of multispectral vs hyperspectral, when using the ML classifier, the spatial resolution of the imagery does affect the accuracy of the classification. A higher spatial resolution allowed for higher classification accuracy.

The WorldView-2 and the PlanetScope classifications resulted with the maximum likelihood as their most accurate classification method, when compared to their unique

classifiers. The AVIRIS hyperspectral was the only remote sensing image that resulted with the unique classifier as the most accurate classification. Comparing the three unique classifiers: SAM resulted in the highest producer accuracy percentage (91%); followed by the OBIA producer accuracy assessment (86%); and the SVM had the least accurate results (83%).

The AVIRIS hyperspectral imagery yielded 91% and 87%, the highest producer accuracy value (SAM) and the third-highest value of the classification (ML). The hyperspectral classification results support the strength of the spectral angle mapper classification algorithm, but they also reveal the maximum likelihood to be a less effective hyperspectral classification algorithm for mapping invasive FAV within the specific aquatic freshwater environment study area. The SAM classifier's ability to analyze 20 bands instead of 3 gave this method an advantage for classifying the distinct pattern of invasive FAV areas. The poorer ML results could possibly be caused by the 3 band MNF subset used (11, 9, 7). For future studies, a higher resolution hyperspectral image might allow for a better hyperspectral ML result. A resolution like the WorldView-2 resolution could possibly result in a more accurate classification, specifically along the class boundaries.

The WorldView-2 multispectral imagery yielded 90% and 86%, the second-best producer accuracy value (ML) and the fourth-best producer accuracy value (OBIA). The high-resolution classification results support the strength of the maximum likelihood classification algorithm. Compared to the other five classification combinations, the OBIA

is not the most effective and accurate classification algorithm, but also was not the worst classification algorithm for mapping invasive FAV within a wetland ecosystem. Regardless of being the fourth most accurate method, OBIA's segmentation ability to classify "objects" based on pixel value and most importantly shape, allowed class boundaries to be persevered and accurately mapped while using OBIA classifier.

The PlanetScope multispectral imagery yielded 85% and 83%, the fifth-best producer accuracy value (ML) and the worst producer accuracy value (SVM). The high-resolution classification results support the strength of the maximum likelihood classification algorithm. Compared to the other five classification combinations, the SVM is not the most effective and accurate classification algorithm for mapping invasive FAV within a wetland ecosystem. Like the other less accurate classifiers, this method poorly mapped the class boundaries. The low accuracy of the Planet/SVM classification reflects the spatial resolution of the PlanetScope sensor as well as the training sample selections being too normally distributed.

Even though all six classifications resulted in producer accuracies between 83% - 91%, there was still error and uncertainty present in all six classifications. The most common classification error that occurred was the misclassification of native vegetation on the boundary between the invasive FAV and the delta water. On the satellite images, the boundary where the water's edge and where the FAV begins is not a hard boundary. Since the spatial resolution for the three satellite images is 1.8m, 2.4m, and 3.7m, there is a gradient from dark black/blue of the delta water to the signature bright red (when using a

false-color infrared band combination) of the invasive FAV mats (Figure 21). These classification errors occur in these areas of darker red pixels. The darker red pixels have a similar reflectance value to the native vegetation that occupies levee islands. This resulted in a false classification of native vegetation, a thin strip of native vegetation surrounding each classified polygon of invasive FAV.

Figure 21. Close-up Planet 3.7m (4, 3, 2 band combination) imagery displaying the gradient from invasive FAV pixel to delta pixels. The pixel values in the middle have similar reflectance values as the natural vegetation.

Out of the four remote sensing classifiers used in this research study, the SAM and OBIA classifiers were able to most accurately classify the boundary between delta water and the invasive FAV, the SVM and ML classifiers least accurately classified this boundary (Figure 22). The WV2 OBIA classification successfully classified the FAV vs. water boundary due to segmentation. The segmentation shape value of 0.2 gave greater importance to pixel color (0.8) during the segmentation process, allowing for a more accurate classification of FAV pixels vs water pixels. The SAM was also able to successfully map the class boundary zones. The SAM compares the angle between the

reference spectra and the pixel, the smaller the angle means the closer the match to the endmember. The small angle of 1.57 radians allowed for the successful classification in class boundary zones.

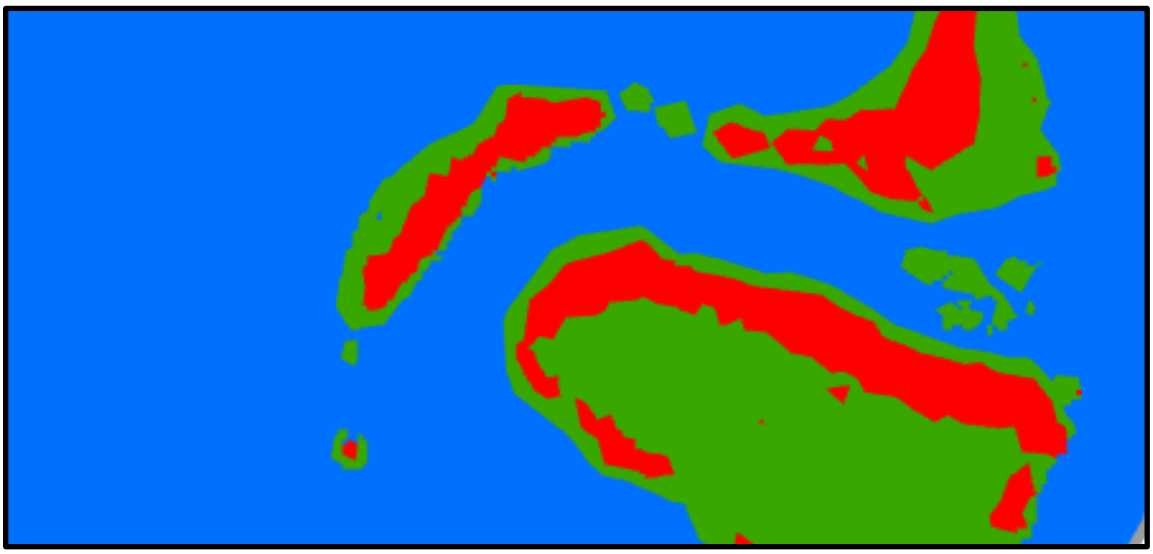

Figure 22. This snapshot from the Planet SVM classification shows the misclassification of native vegetation on the boundary between the invasive FAV and the delta water.

Both the maximum likelihood and the support vector machine classifiers misidentified native delta vegetation where in reality there were FAV mats in contact with open delta water. The WV2 and AVIRIS ML classifications were able to more accurately classify this boundary compared to the lower resolution Planet ML. The higher resolutions of the AVIRIS and WorldView-2 (2.4m & 1.8m) allowed for the gradient between the water and invasive FAV mats to not have as an intense gradient color change, which allowed a more accurate classification result. The Planet ML had similar misclassification errors as the Planet SVM. These errors were likely caused by the 3.7m resolution of the

imagery. Implementing more training sites or increasing spatial resolution could help reduce classification error for the ML and SVM classifiers.

The CA Department of Boating and Waterways contracts out their mapping of invasive FAV in the delta to a commercial environmental consulting firm called BioBase. BioBase creates their classification maps of floating aquatic vegetation using a cloud-based mapping algorithm called EcoSat. EcoSat is a semi-automated processing of high-resolution satellite images to map floating aquatic vegetation in wetlands and waterbodies greater than 25 kilometers squared. EcoSat algorithms are calibrated for Digital Globe WorldView (2, 3, and 4), Airbus Pléiades, and European Space Agency (ESA) Sentinel 2 satellite sensors (BioBasemaps, 2018). BioBase's EcoSat uses algorithms, similar to the OBIA method, to define discrete areas and boundaries of different vegetation communities. These polygon "objects" are automatically given unique classification numbers. BioBase allows their customers to have control over what to name the objects or whether to delete or lump classifications and reprocess the image and data with the new classifications. Shapefiles and raw imagery, that are often hundreds of megabytes, are uploaded and processed by BioBase's cloud-based servers. BioBase's average turnaround time from imagery tasking order to delivery of results is 60 days. Comparing BioBase's EcoSat method with the six imagery/methods combinations used in this invasive FAV research study, the EcoSat and OBIA classification methods resulted with the best preservation of landcover boundaries for both BioBase and this research study. The results from this invasive FAV research study support BioBase's decision to use an object-based

classification method combined with high resolution multispectral aerial imagery for mapping multiple vegetation landcover.

In order to more thoroughly research the most effective imagery/classification combination for mapping and identifying invasive FAV within an aquatic freshwater ecosystem, future studies should acquire different satellite imagery from the same year. If all three images of the central delta study area were flown during the same month and year, there would only be one set of ground-truthed GPS training and validation points for all six classifications/ imagery combinations. This would have allowed for more precise and comparable classifications and producer accuracy assessments. Unfortunately, for this research study, WorldView-2 multispectral and AVIRIS hyperspectral satellite imagery from August 2019 were not available, only the multispectral PlanetScope imagery was available. PlanetScope's multispectral imagery is the most up-to-date imagery out of the three satellite images used. Planet usually releases new imagery on a weekly basis. WorldView-2 imagery is updated annually. The only available image that was flown during the invasive FAV bloom period, and was within the study area boundary, was from August of 2018. For the AVIRIS hyperspectral imagery, available images for download are only posted to the free JPL data portal if a past research project contracts out an AVIRIS flight. For this research study, the only image that was within the central delta study area and fit within the FAV bloom time frame was from a 2007 delta research project. Contracting out new flights for both WorldView-2 and AVIRIS would become extremely costly.

For this research project, with a limited budget for satellite imagery, the decision was made to acquire imagery from different years, but to choose imagery within the same temporal time frame of August. Due to this decision, the differences between the three satellite imagery types used for this research study affect the overall accuracy assessment comparison.

6. Conclusion

This research study investigated the most effective remote sensing method of classifying invasive floating aquatic vegetation species by comparing three different types of satellite imagery data: high resolution multispectral; very high resolution multispectral; and hyperspectral; as well as four different classification methods: maximum likelihood; spectral vector machine; spectral angle mapper; and object-based imagery analysis. This comparison of methods / imagery type would be more accurate and truly comparable if instead all three images were flown during the same month/year, using the same training samples and accuracy assessment samples. This decision accounts for the possible effects of variation in classification method accuracies.

The spectral angle mapper classification / hyperspectral AVIRIS imagery resulted in the most effective imagery type / classification algorithm combination for accurately identifying and classifying invasive FAV in the Central Sacramento Delta. The support vector machine classification / multispectral PlanetScope satellite imagery resulted in the

least effective satellite imagery classification algorithm combination for identifying and classifying invasive FAV in the Central Sacramento Delta.

Based on the ML classifier comparison, very-high resolution multispectral WorldView-2 (1.8m) imagery is the most effective for the identification of invasive FAV, followed by the high resolution AVIRIS hyperspectral (2.4m) imagery, and finally the high resolution multispectral Planet (3.7m) imagery. These results revealed that spatial resolution does affect classification accuracy, meaning the higher the resolution, the better the results will be.

The results from this research study revealed the decision between using hyperspectral vs multispectral may be a more important than deciding between different classification algorithms. If hyperspectral imagery is available, the most effective remote sensing classification algorithm for identifying invasive floating vegetation in Central Delta aquatic freshwater ecosystem is the spectral angle mapper classifier, followed by the maximum likelihood. If only multispectral imagery is available, the most effective supervised classification remote sensing algorithm for classifying invasive vegetation in central delta aquatic freshwater ecosystem is the maximum likelihood classifier, followed by the OBIA, then SVM.

In terms of errors and misclassification, this research study revealed that the spatial resolution of an image is an important factor for minimizing error. This research study also concluded that the OBIA may be the best classification algorithm for minimizing boundary

errors in multispectral analysis, and the spectral angle mapper may be best for reducing boundary misclassifications for hyperspectral analysis.

References

Abdel-Rahman, E. M., Mutanga, O., Adam, E., & Ismail, R. (2014). “Detecting Sirex noctilio grey-attacked and lightning-struck pine trees using airborne hyperspectral data, random forest and support vector machines classifiers”. *ISPRS Journal of Photogrammetry and Remote Sensing*, *88*, 48–59. doi: 10.1016/j.isprsjprs.2013.11.013

Adam, E., Mutanga, O., & Rugege, D. (2010). “Multispectral and hyperspectral remote sensing for identification and mapping of wetland vegetation: a review”. *Wetlands Ecology and Management*, *18*(3), 281–296. doi: 10.1007/s11273-009-9169-z

Agjee, N. E., Mutanga, O., & Ismail, R. (2015). “Remote sensing bio-control damage on aquatic invasive alien plant species”. *South African Journal of Geomatics*, *4*(4), 464. doi: 10.4314/sajg.v4i4.8

Ashraf, S., Brabyn, L., Hicks, B. J., & Collier, K. (2010). “Satellite remote sensing for mapping vegetation in New Zealand freshwater environments: A review”. *New Zealand Geographer*, *66*(1), 33–43. doi: 10.1111/j.1745-7939.2010.01168.x

Bazi, Y., Melgani, F. (2007). “Semisupervised PSO-SVM Regression for Biophysical Parameter Estimation”. *IEEE Transactions on Geoscience and Remote Sensing*, *45*(6), 1887–1895. doi: 10.1109/tgrs.2007.895845

Belluco, E., Camuffo, M., Ferrari, S., Modenese, L., Silvestri, S., Marani, A., & Marani, M. (2006). “Mapping salt-marsh vegetation by multispectral and hyperspectral remote sensing”. *Remote Sensing of Environment*, *105*(1), 54–67. doi: 10.1016/j.rse.2006.06.006

BioBasemaps. (2018). “Training EcoSat Vegetation Classifications”. *BioBasemaps*. https://blog.biobasemaps.com/2018/08/15/training-ecosat-vegetation-classifications-user-tips/#more-22.

Bossard, C. C., Randall, J. M., & Hoshovsky, M. C. (Eds.). (2000). “Invasive Plants of Californias Wildlands”. *Taxon*, *50*(2), 627. doi: 10.2307/1223915

Boyer K, Sutula M. (2015). “Factors controlling submerged and floating macrophytes in the Sacramento–San Joaquin Delta”. *Central Valley Regional Water Quality Control Board and California Environmental Protection Agency State Water Resources Control Board*. http://online.sfsu.edu/katboyer/Boyer_Lab/Publications_files/Boyer%20and%20Sutula%2010.07.15%20Final.pdf

California State Parks, State of California (2018). “Floating Aquatic Vegetation”. *CA Dept. of Boating and Waterways*. http://dbw.parks.ca.gov/?page_id=28995.

California State Parks, State of California (2019). “PUBLIC NOTICE: 2019 Floating Aquatic Vegetation Control Program”. *CA Dept of Boating and Waterways*. http://dbw.parks.ca.gov/pages/28702/files/PUBLIC%20NOTICE%202019%20FAV%20Control%20Program%20with%20Maps%20FINAL.pdf

Cohen, A. N., & Carlton, J. T. (1995). “Nonindigenous aquatic species in a United States estuary: A case study of the biological invasions of the San Francisco Bay-Delta” (pp. 238): *United States Fish and Wildlife Service National Sea Grant College Program.*

Cohen, A. N., & Carlton, J. T. (1998). “Accelerating invasion rate in a highly invaded estuary”. *Science*, 279, 555−558. doi: 10.1126/science.279.5350.555

Dandelot, S., Verlaque, R., Dutartre, A., & Cazaubon, A. (2005). “Ecological, Dynamic and Taxonomic Problems Due to Ludwigia (Onagraceae) in France”. *Hydrobiologia, 551*(1), 131–136. doi: 10.1007/s10750-005-4455-0

Deloach, CJ. Everitt, JH. Yang, C. (2005). “Remote Sensing of Giant Reed with QuickBird Satellite Imagery”. *Journal of Aquatic Plant Management*. Vol 43. doi:10.1117/1.3148866

Dennison WC, Orth RJ, Moore KA, Stevenson JC, Carter V, Kollar S, Bergstrom PW, Batiuk RA. (1993) “Assessing water quality with submerged aquatic vegetation”. *BioScience, 43*(2), 86-94. doi:10.2307/1311969

DiPietro, Deanne. Ustin, Susan. Underwood, Emma. 2002. “Mapping the Invasive Plant Arundo Donax and Associated Riparian Vegetation Using AVIRIS”. *Center for Spatial Technologies and Remote Sensing (CSTARS) Department of Land, Air, and Water Resources, University of California*.

Govender, M. Chetty, K. Bulcock, H. (2007) “A review of hyperspectral remote sensing and its application in vegetation and water resource studies”. *Journal of Water South Africa*. *33*(2). doi: 10.4314/wsa.v33i2.49049

Haury, J., Druel, A., Cabral, T., Paulet, Y., Bozec, M., & Coudreuse, J. (2014). “Which adaptations of some invasive Ludwigia spp. (Rosidae, Onagraceae) populations occur in contrasting hydrological conditions in Western France?”. *Hydrobiologia, 737*(1), 45–56. doi: 10.1007/s10750-014-1815-7

Hawkes, Alison. (2014). “Water Hyacinth Thrives in Drought-Stricken Delta”. *Bay Nature Magazine*. https://baynature.org/article/water-hyacinth-thrives-drought-stricken-delta/

Hestir, Erin. Khanna, Shruti. Margaret, Andrew. Rajapakse, Sepalika. Santos, Maria. Ustin, Susan. Viers, Joshua. (2008). “Identification of invasive vegetation using hyperspectral remote sensing in the California Delta ecosystem”. *Remote Sensing of Environment*, *112*(11), 4034–4047. doi: 10.1016/j.rse.2008.01.022

Huang, H., Gong, P., Clinton, N., Hui, F. (2008). “Reduction of atmospheric and topographic effect on Landsat TM data for forest classification”. *International Journal of Remote Sensing*, *29*(19), 5623–5642. doi: 10.1080/01431160802082148

Johnson, Brian. Roberts, Charles. Xie, Zhixiao. (2008). “Object-based target search using remotely sensed data: A case study in detecting invasive exotic Australian Pine in south Florida”. *ISPRS Journal of Photogrammetry and Remote Sensing*, *63*(6), 647–660. doi: 10.1016/j.isprsjprs.2008.04.003

Khanna, S., Santos, M. J., Ustin, S. L., & Haverkamp, P. J. (2011). “An integrated approach to a biophysiologically based classification of floating aquatic macrophytes”. *International Journal of Remote Sensing*, *32*(4), 1067–1094. doi: 10.1080/01431160903505328

Khanna, S., Santos, M. J., Boyer, J. D., Shapiro, K. D., Bellvert, J., & Ustin, S. L. (2018). “Water primrose invasion changes successional pathways in an estuarine ecosystem”. *Ecosphere*, *9*(9). doi: 10.1002/ecs2.2418

Kokaly, R. F., Despain, D. G., Clark, R. N., & Livo, K. (2003). “Mapping vegetation in Yellowstone National Park using spectral feature analysis of AVIRIS data”. *Remote Sensing of Environment*, *84*(3), 437–456. doi: 10.1016/s0034-4257(02)00133-5

Lee, K., Lunetta, R. (1996). “Wetland detection methods”. *Wetland and environmental application of GIS* (pp. 249–284)

Li, L., Ustin, S. L., & Lay, M. (2005). “Application of multiple endmember spectral mixture analysis (MESMA) to AVIRIS imagery for coastal salt marsh mapping: a case study in China Camp, CA, USA”. *International Journal of Remote Sensing*, *26*(23), 5193–5207. doi: 10.1080/01431160500218911

Lund, J., Hanak, E., Fleenor, W., Howitt, R., Mount, J., & Moyle, P. (2007). "Envisioning Futures for the Sacramento–San Joaquin Delta ". *San Francisco: Public Policy Institute of California*, pp .324. doi: 10.1525/california/9780520261976.001.0001

Mack, R.N., Simberloff, D., Lonsdale, W.M., Evans, H., Clout, M. and Bazzaz, F.A., (2000). "Biotic invasions: Causes, epidemiology, global consequences, and control". *Ecological Applications*, Vol.10 (3), p.689-710. doi: 10.1890/1051-0761(2000)010[0689:BICEGC]2.0.CO;2

Mantero, P., Moser, G., & Serpico, S. (2005). "Partially Supervised classification of remote sensing images through SVM-based probability density estimation". *IEEE Transactions on Geoscience and Remote Sensing*, *43*(3), 559–570. doi: 10.1109/tgrs.2004.842022

Mountrakis, G., Im, J., & Ogole, C. (2011). "Support vector machines in remote sensing: A review". *ISPRS Journal of Photogrammetry and Remote Sensing*, *66*(3), 247–259. doi: 10.1016/j.isprsjprs.2010.11.001

Pande-Chhetri, R., Abd-Elrahman, A., Liu, T., Morton, J., & Wilhelm, V. L. (2017). "Object-based classification of wetland vegetation using very high-resolution unmanned air system imagery". *European Journal of Remote Sensing*, *50*(1), 564–576. doi: 10.1080/22797254.2017.1373602

Pimentel, D., Lach, L., Zuniga, R., & Morrison, D. (2000). "Environmental and Economic Costs of Nonindigenous Species in the United States". *BioScience*, *50*(1), 53. doi: 10.1641/0006-3568(2000)050[0053:eaecon]2.3.co;2

Toft, J. D., Simenstad, C. A., Cordell, J. R., & Grimaldo, L. F. (2003). "The effects of introduced water hyacinth on habitat structure, invertebrate assemblages, and fish diets". *Estuaries*, *26*(3), 746–758. doi: 10.1007/bf02711985

Underwood, E. C., Mulitsch, M. J., Greenberg, J. A., Whiting, M. L., Ustin, S. L., & Kefauver, S. C. (2006). "Mapping Invasive Aquatic Vegetation in the Sacramento- San Joaquin Delta using Hyperspectral Imagery". *Environmental Monitoring and Assessment*, *121*(1-3), 47–64. doi: 10.1007/s10661-005-9106-4

Ustin, S. L., Greenberg, J. A., Hestir, E. L., Khanna, S., Santos, M. J., Andrew, M. E., Whiting, M., Rajapakse, S., & Lay, M. (2006). "Mapping invasive plant species in the Sacramento–San Joaquin Delta using hyperspectral imagery". *Sacramento, CA: Department of Boating and Waterway: Aquatic Weed Control.* (pp. 92)

Zhang, L., Wang, M.-H., Hu, J., & Ho, Y.-S. (2010). “A review of published wetland research, 1991–2008: Ecological engineering and ecosystem restoration”. *Ecological Engineering*, *36*(8), 973–980. doi: 10.1016/j.ecoleng.2010.04.029